

Plasticity based approach for cyclic behaviour of Unreinforced Masonry

K.Sravani

A Thesis Submitted to
Indian Institute of Technology Hyderabad
In Partial Fulfillment of the Requirements for
The Degree of Master of Technology



Department of Civil Engineering

June 2015

Declaration

I declare that this written submission represents my ideas in my own words, and where ideas or words of others have been included, I have adequately cited and referenced the original sources. I also declare that I have adhered to all principles of academic honesty and integrity and have not misrepresented or fabricated or falsified any idea/data/fact/source in my submission. I understand that any violation of the above will be a cause for disciplinary action by the Institute and can also evoke penal action from the sources that have thus not been properly cited, or from whom proper permission has not been taken when needed.

K. Sravani
(K. SRAVANI)

(Signature)

(K.Sravani)

CE13M1003

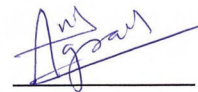
(Roll No.)

Approval Sheet

This Thesis entitled Plasticity based approach for cyclic behaviour of Unreinforced Masonry by Kondapalli Sravani is approved for the degree of Master of Technology from IIT Hyderabad



(Dr. Saswata Battacharya) Examiner
Dept. of Mat Science and Eng IITH



(Dr. Anil Agarwal) Examiner
Dept. of Civil Eng IITH

 10/27/15

(Dr. Amirtham Rajagopal) Adviser
Dept. of Civil Eng
IITH

Acknowledgements

I would like to express my deepest gratitude to my advisor Dr. Raja Gopal for his guidance and support. His extreme interest in the research is a constant source of motivation for me. He is a great person and one of the best mentors, I always be thankful to him. I would also like to thank Dr. Manoj Pandey for devoting his time in discussing ideas with me and giving his invaluable feedback. I would like to thank all my Adviser group mates for making our lab such a great place to work. Thanks to my M.Tech class mates for teaching me lots of project related things. I would like to thank my amazingly loving and supportive parents and my brother and my friend who have always been with me.

Abstract

In present Thesis a plasticity based composite interface model is proposed for the simulation of cyclic behavior of the masonry under cyclic loading. The monotonic composite interface model consist of single surface yield criterion which is extension of mohr-Coulomb criteria with cut in tension region and a cap in compression region. The inelastic behavior of Interface include the softening of the tensile strength, cohesion, frictional angle and dilation angle, whereas for compression hardeningis considered and Nonlinearity in unloading/reloading is introduced in case of cyclic loading . The interface model is implemented in standard finite element software (ABAQUS) by using user defined subroutine .Two Unloading yield surfaces are introduced in the existing monotonic Model which are driven by Mixed hardening rule. Evolution laws based on phenomenological data are used for modelling unloading to compression and to tension separately

Contents

Declaration	ii
Approval Sheet	iii
Acknowledgements	iv
Abstract	v
Nomenclature	vii
1 Introduction	1
1.1 Introduction	1
2 Literature Review and Objectives	4
2.1 Objectives of the thesis	5
3 Masonry: Material Description	6
3.1 Introduction	6
3.2 Softening behaviour aspects	7
3.2.1 Tensile strength softening	7
3.2.2 Compressive strength softening	8
3.2.3 Shear strength softening	8
3.3 Property of masonry constituents	8
3.3.1 Masonry units	8
3.3.2 Mortar	9
3.3.3 Property of unit-mortar interfaces	9
4 Modelling Strategies of Masonry	13
4.1 Different modelling strategies for masonry	13
4.1.1 Modelling with FEM	13
4.2 Modelling with interface elements	15
4.3 Modelling with DEM	15
4.4 Material and structural behavior of masonry	16
4.4.1 Limit analysis	17
4.4.2 Equivalent strut	17
4.4.3 Macro-elements: equivalent models and frame models title	18

5	The Constitutive Model for Cyclic loading	20
5.1	The Constitutive Model for Cyclic loading	20
5.1.1	Elastic behaviour	21
5.1.2	Plastic behaviour	21
5.1.3	Unloading or Reloading to tension	21
5.1.4	Unloading or Reloading to Compression	22
5.1.5	Mixed Hardening Law	23
5.1.6	Evolution laws	23
5.1.7	Unloading Yield Surfaces	26
5.1.8	Characteristics of unloading surfaces	26
5.1.9	Possible Cyclic loading movements of the Constitutive Model	27
5.1.10	Hardening laws adopted for unloading Cases	27
5.1.11	Evolution of hardening parameters	27
5.1.12	Elastic-plastic tangent modulus	28
5.1.13	Algorithmic aspect of local and global solver	29
5.2	Appendix	33
5.2.1	Yield Function	33
5.2.2	Potential Function	33
5.2.3	Derivatives	33
5.2.4	Jacobian Terms	34
5.2.5	Algorithmic Implementation	38
6	Verification Examples	41
6.1	Verification Examples for Monotonic Loading	41
7	Applications of proposed Model	44
7.1	Behavior of Interface during cyclic loading	44
7.1.1	Behavior Of Interface in uniaxial Tension and Compression	45
7.2	Direct shear test	45
7.3	Behavior of a two Brick model in Monotonic and Cyclic loading	46
7.3.1	Monotonic Behavior	47
7.3.2	Cyclic behavior of a two brick model	47
7.4	UPC stacked bond prisms	50
7.4.1	Masonry and Interface properties adopted for Brick prism	50
7.5	Summary and Conclusions	52
8	References	53
8.1	References	53

Chapter 1

Introduction

1.1 Introduction

Masonry is the building of structures from individual units laid in and bound together by mortar. The term masonry may sometime also refer to the units themselves. The common materials of masonry construction are brick, stone, marble, granite, travertine, limestone, cast stone, concrete block, glass block, stucco, and tile. Masonry structures have found widespread applications around the world for centuries. In old buildings masonry construction was used as load bearing members of the structure. There has been large use of the masonry in recent years as an infill in concrete and steel frames. The behaviour of masonry is very complex and highly non-linear due to the behaviour of its constituents i.e. brick and mortar, which are quasi-brittle in nature and have the large difference in their stiffness. A large number of possible combinations can be obtained by the variation of geometry, nature and arrangement of mortar and brick. In the recent years with advances in computation mechanics, it has been possible to simulate the complex behaviour of masonry.

Many computational studies have been carried out at various scales to understand and simulate the behaviour of the masonry. These include: micro-, macro- and meso-scale analysis. The micro scale analysis require significant computational time. However, the micro scale analysis is able to predict accurate behaviour of the structure that account for the nonlinear behaviour of the material constituent failure.

Most heritage structures, including monuments of huge architectural and historical value are made up of masonry construction. Many of them are located in earthquake prone sites. Thus it is important to evaluate the existing building in order to guarantee the safety of people as well as to conserve the architectural heritage. Failure analysis of masonry thus become important to evaluate strength of the existing building and to provide the strengthening solutions for the designer of the new building. The analysis of masonry structures is a complex task. The material presents a very particular mechanical behaviour, which is principally due the lack of homogeneity and standardization. The structural response of such a composite material derives from the complex interaction between units and mortar joints. Masonry is periodic heterogeneous and anisotropic structure and exhibits directional property due to influence of the mortar. Under the in-plane loading, all type of masonry is subjected to biaxial stress and thus masonry constituent may fail in individual or combined mechanisms.



Figure 1.1: A earthquake-damaged Unreinforced Masonry building with an out of plane collapse in Italy Photo courtesyRoberto Serra/Iguana Press/Getty



Figure 1.2: A earthquake-damaged building in Northern Italy ,in 2012 , Photo courtesyRoberto Serra/Iguana Press/Getty



Figure 1.3: Daraharatower during Nepal earthquake Photo courtesy colinDaileda

Un-reinforced brick masonry (URM) has been the widely used construction materials for buildings in most of the places in India due to their availability and the ease in construction practice . Most of the traditional buildings were also constructed in mud mortar and different locally available material. Brick masonry is still one of the most popular construction materials with cement sand mortar despite of its low tensile strength .The recent earthquakes in Nepal and India proved that both the newer and older masonry building are highly vulnerable to the earthquake

Chapter 2

Literature Review and Objectives

Extensive Literature review was done and salient features are mentioned here. Based on the sought accuracy level, different types of computational methods, with varying levels of computational demand, have been presented to assess the behavior of masonry structures under static and dynamic loadings [1,2,8,9]. Pasticier et al. [10] used a very simple macro-element model to perform two-dimensional seismic analysis of masonry panels, where each part was divided into smaller panels that were represented by an equivalent beam element with predefined hysteretic behavior. Chen et al. [11] used nonlinear shear springs in series with rotational springs to simulate both shear and flexural in-plane response of masonry walls; proposed macro-element includes an axial spring, three shear springs, and two rotational springs to simulate the behavior of masonry walls using large rigid elements and springs attached between them. Casolo [12] developed a macro scale model where he compared the frequencies and mode shapes of a masonry wall using his proposed model and finite element mode. Park et al. [8] proposed a model in which a masonry panel was divided into a number of springs with different hysteresis loops. Page [14] suggested using interface elements between bricks that yield surface in this particular interface model is only defined for tensile and shear failure. Lourenco [1] subsequently modified Page's model by adding a compressive cap to the yield surface, which led to accounting for crushing of the masonry bricks. Oliveira and Lourenco [2] later generalized Lourenco's model to allow the assessment of the cyclic behavior of masonry walls subjected to in-plane loading. In the model proposed by Lourenco [1] and later by Oliveira and Lourenco [2], bricks are modeled using elastic elements, and the nonlinear behavior of the interface elements includes the tensile, shear and compression failures [1]. Dolatshahi and Aref [15] presented a meso-scale numerical model for simulation of crack propagation in unreinforced masonry walls using rigid elements in combination with interface elements. Using rigid elements that replaced solid elements in the FEM have led to significantly decreasing the number of degrees-of-freedom (DOF). Karapitta et al. [17] used a homogenization technique within an explicit formulation to capture the cyclic behavior of in-plane masonry panels; very few 3D cyclic finite element models are readily available to accurately model the behavior of masonry structures. Amjad J. Aref et al used 3D cyclic meso-scale numerical procedure for simulation of unreinforced masonry structures using VUMAT structures

2.1 Objectives of the thesis

The Thesis is based on the work that aims mainly towards achieving these objectives

- 1.To propose and develop a constitutive micro model for unreinforced masonry which includes Nonlinear behavior under cyclic loading in Tension and Compression
- 2.To Trace the structural response through post peak behavior in Masonry under cyclic loading
- 3.To perform a numerical study to validate the model by comparing the predicted behavior with the behavior observed in experiments

Chapter 3

Masonry: Material Description

3.1 Introduction

Masonry is the building of structures from individual units laid in and bound together by mortar. The term masonry can also refer to the units themselves. The common materials of masonry construction are brick, stone, marble, granite, travertine, limestone, cast stone, concrete block, glass block, stucco, and tile. Generally, masonry is highly durable form of construction. However, the materials used, the quality of the mortar and workmanship, and the pattern in which the units are assembled can significantly affect the behaviour and durability of the overall masonry construction

Masonry is a heterogeneous anisotropic continuum. In particular, the inhomogeneity is due to the different mechanical properties of its constituents. Anisotropy is due to the different masonry patterns, that can be obtained by variation of geometry, nature and arrangement of mortar and brick. The behaviour of masonry is very complex and highly non-linear due to the behaviour of its constituents, which are quasi-brittle in nature. Thus for micro-modelling, a material description must be obtained from experimental tests on the masonry constituents. For macro-modelling, a small tests must be performed on masonry specimens of sufficient size under homogeneous states of stress or strain, to obtain average stress-strain relationship (Importance is given to deformation controlled test, because it is capable of capturing the entire load-displacement diagram). As a alternative to experiments, these average stress-strain relationships can be obtained from the homogenization. The complete description of the material is not pursued in this study.

The property of masonry depends up on the large no of factors, such as material properties of the units and mortar; arrangement of units; anisotropy of units; dimension of units; joint thickness; quality of workmanship; degree of curing; environment and age etc. Because of these large number of variable, the masonry research community showing the interest in the sophisticated numerical models from last two decades. Moreover, numerical models required the reliable experimental data. The experimental data are required for test parameters and for the comparisons and conclusions. It is a usual practice to report and measure only strength values. In particular, masonry shows the softening behaviour after peak value. Thus it is very important to retrieve the information of post-peak or softening regime. But very rare information was available in the literature about the softening regime of the masonry and its constituents. Thus, in the following chapter the aspects of softening behaviour is explain before the brief description of masonry and its constituent is given.

3.2 Softening behaviour aspects

Masonry shows the softening behaviour in the post peak region. It is typical due to quasi-brittle nature of its constituent i.e. brick and mortar. Softening defined as a gradual decrease of mechanical resistance under a continuous increase of deformation. It happened due to the present of progressive internal micro crack. Such mechanical behaviour is commonly attributed to the heterogeneity of the material, due to the presence of different phases and material defects, like flaws and voids. Even prior to loading the structure, mortar contains microcracks due to the shrinkage during curing and the presence of the aggregate. The clay brick contains inclusions and microcracks due to the shrinkage during the burning process. Initially, these microcracks are stable which means that they grow only when the load is increased. During the initial loading the cracks remains stable and number of new crack formation is very less. But, around peak load an acceleration of crack formation takes place and the formation of macrocracks starts. The macrocracks are unstable, which means that the load has to decrease to avoid an uncontrolled growth. In a deformation controlled test the macrocracks growth results in softening and localization of cracking in a small zone while the rest of the specimen unloads. It is assumed that the inelastic behaviour can be described by the integral of the $\sigma - \delta$ diagram. These crack can opened in different mode i.e. fracture energy mode I for tensile loading, fracture energy mode II for shear loading and compressive fracture energy.

3.2.1 Tensile strength softening

The phenomenon of tensile failure has been well identified, see Figure . The inelastic behaviour of tensile strength degradation is described by the integral of the $\sigma - \delta$ diagram. This quantity is the tensile fracture energy (G_f), and it is defined as the amount of energy to create a unitary area of a crack opening.

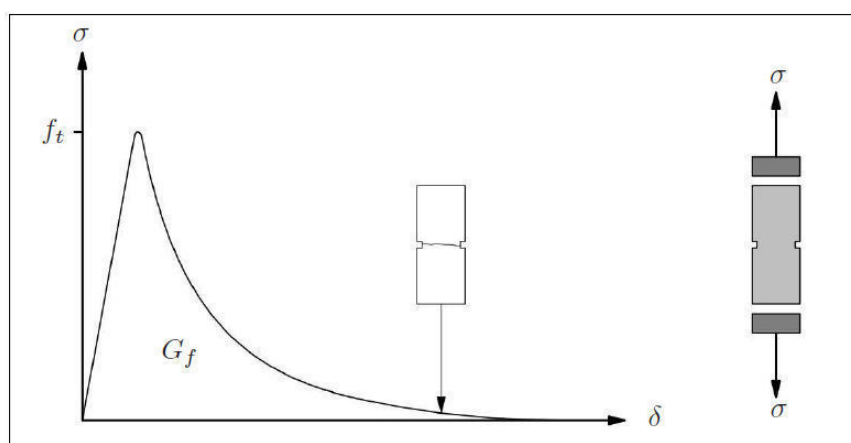


Figure 3.1: Behaviour of quasi-brittle material under uniaxial tensile loading and definition of tensile fracture energy (f_t denotes tensile strength)lourencco1996.[1]

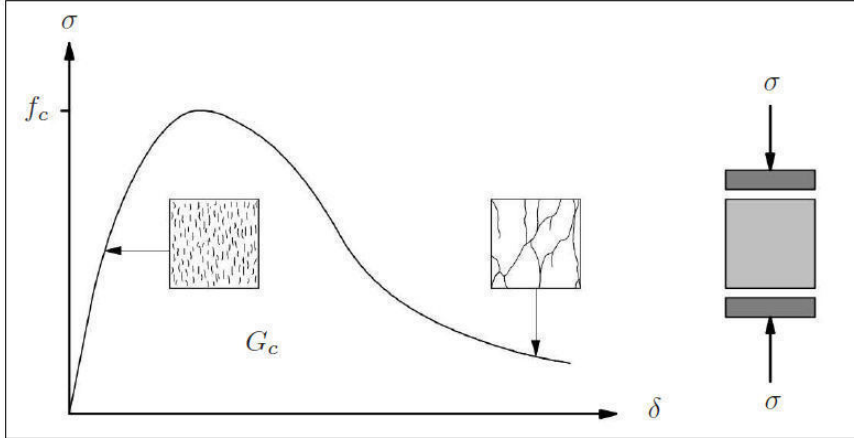


Figure 3.2: Behaviour of quasi-brittle material under uniaxial compressive loading and definition of compressive fracture energy (f_c denotes compressive strength) lourencco1996.

3.2.2 Compressive strength softening

In the compressive failure, softening behaviour is highly dependent upon the boundary conditions in the experiments and the size of the specimen. Experimental concrete data provided by Vonk [?] indicated that the behaviour in uniaxial compression is governed by both local and continuum fracturing processes. Similar to tension, the inelastic behaviour of compression strength is described by the integral of the $\sigma - \delta$ diagram, see Figure 3.1. Now, this quantity is the compressive fracture energy (G_c). It has the same notion as the tensile fracture energy (G_f), because the underlying failure mechanisms are identical, viz. continuous crack growth at micro-level.

3.2.3 Shear strength softening

In the shear failure, a softening behaviour is observed as degradation of the cohesion in Coulomb friction models. It represents the mode II failure mechanism, that consists of slip of the unit-mortar interface under shear loading. Again, it is assumed that the inelastic behaviour is described by the mode II fracture energy G_f^{II} , defined by the integral of the $\tau - \delta$ diagram in the absence of normal confining load, see Figure 3.3.

3.3 Property of masonry constituents

The property of masonry dependants up on the property of its constituents. Thus, it is important to know the property of brick, mortar and unit-mortar interface for studying the masonry. Generally, compression strength test are used for indication the quality of the material.

3.3.1 Masonry units

For the masonry units, a standard tests with solid platens have being done for compressive strength as per IS 3495 part 1. The test results in an artificial compressive strength due to the restraint effect in its lateral direction. The effect can be minimizes by normalizing the compressive strength, by

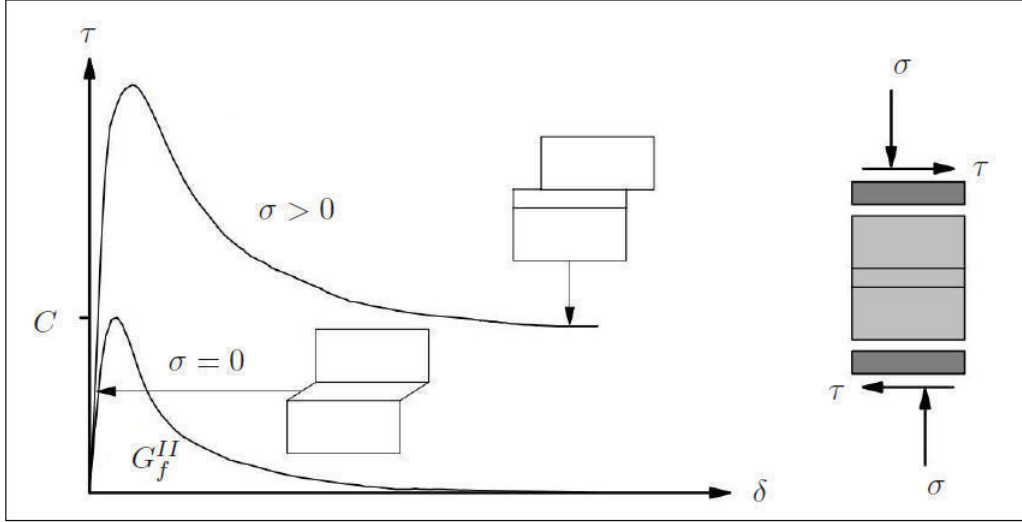


Figure 3.3: Behaviour of masonry under shear and definition of mode II fracture energy (C denotes cohesion)

multiplying with appropriate shape/size factor. No experiments in the uni-axial post-peak behaviour of compressed bricks and blocks exists, therefore, no information about the compressive fracture energy G_c can be obtain.

Even though, It is difficult to relate the tensile strength of the masonry unit to its compressive strength due to the different shapes, materials, manufacture processes and volume of perforations. Many researcher conducted extensive testing to obtained a ratio between the tensile and compressive strength. Schubert (1994)[13] find ratio ranges from 0.03 to 0.10 for clay, calcium-silicate and concrete units. For the fracture energy G_f of solid clay and calcium-silicate units, both in the longitudinal and normal directions. Van der Pluijm [14] found fracture energy values ranging from 0.06 to 0.13 [Nmm/mm^2] for tensile strength values ranging from 1.5 to 3.5 [N/mm^2].

3.3.2 Mortar

The compressive strength of is obtained from standard tests carried out on the cube of 75 [mm] as per IS 4031 part-7 1998. Moreover, investigations in mortar disks extracted from the masonry joints has being carried out to fully characterize the mortar behaviour, Bierwirth et al. (1993), Schubert and Hoffman (1994) and Stöckl et al.(1994). Nevertheless, there is still a lack of knowledge about the complete mortar uni axial behaviour in tension and compression.

3.3.3 Property of unit-mortar interfaces

The bond between the unit and mortar is most critical part of the masonry and governs most non-linear response of the joints. Moreover, it is the weakest link in masonry assemblages. Predominately two failure phenomena can be considered for unit-mortar interface, one associated with tensile failure (mode I) and the other associated with shear failure (mode II).

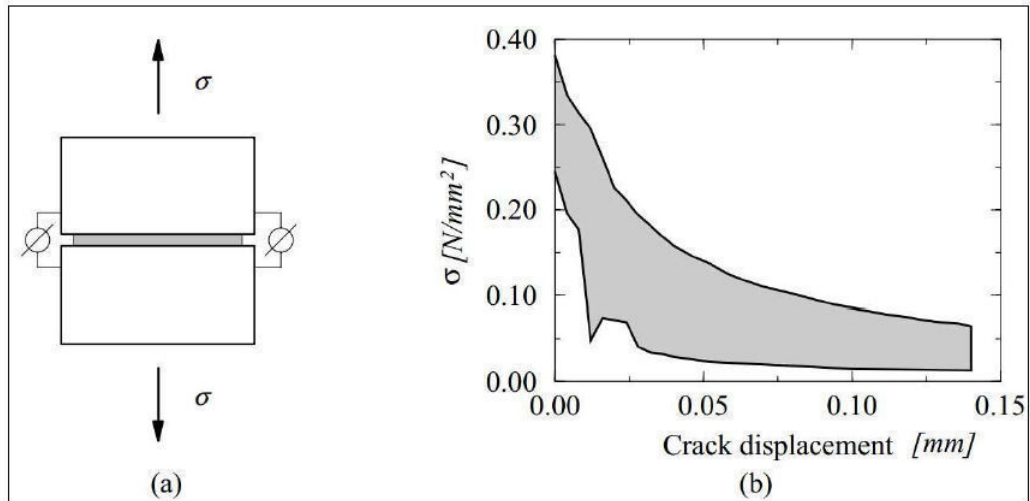


Figure 3.4: Tensile bond behaviour of masonry (pluijm1992,pluijm1993): (a) test specimen; (b) typical experimental stress-crack displacement results for solid clay brick masonry.

Mode I failure

Van der Pluijm (pluijm1992,pluijm1993)[13,14] carried out deformation controlled tests in series. The test was conducted on small masonry specimens made up of solid clay and calcium-silicate units. These tests resulted in an exponential tension softening curve with a mode I fracture energy G_f^I , see Figure 3.4(a).

During the first series in 1990, it becomes clear by close observation of the cracked specimens, that the bond area was smaller than the cross sectional area of the specimens. This net bond surface area seems to concentrate in inner part of the specimen. The reduction in bond area is a combined result from shrinkage of the mortar and the process of laying units in the mortar bed joint. In many cases the net bond surfaces area was restricted to central part of the specimen. Therefore, it is assumed that the reduction of the bond surfaces is caused by the edges of the specimen. With this assumption, it is possible to estimate the fracture energy. Hence, the net bond surface area must be corrected according to the number of edges, see Figure 3.5.

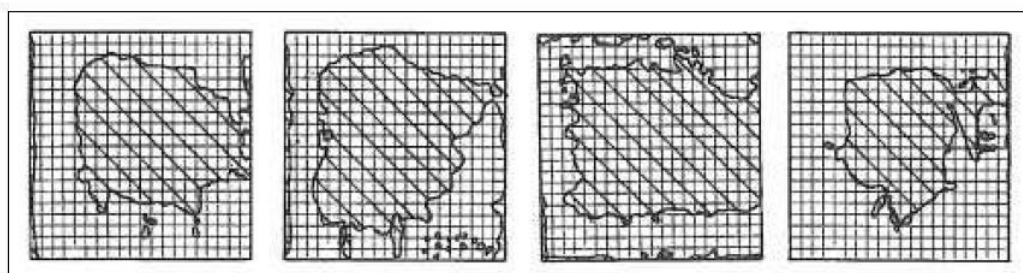


Figure 3.5: Tensile bond surface [?] typical net bond surface area for tensile specimens of solid clay units.

Mode II failure

For capturing the shear response of masonry joints experimentally. It is very important to set-up a uniform state of stress in the joints. But it very is difficult, because the equilibrium constraints introduce non-uniform normal stresses in the joints. For the detailed study readers are referred to Atkinson *et al.* [15] and Van der Pluijm [14]

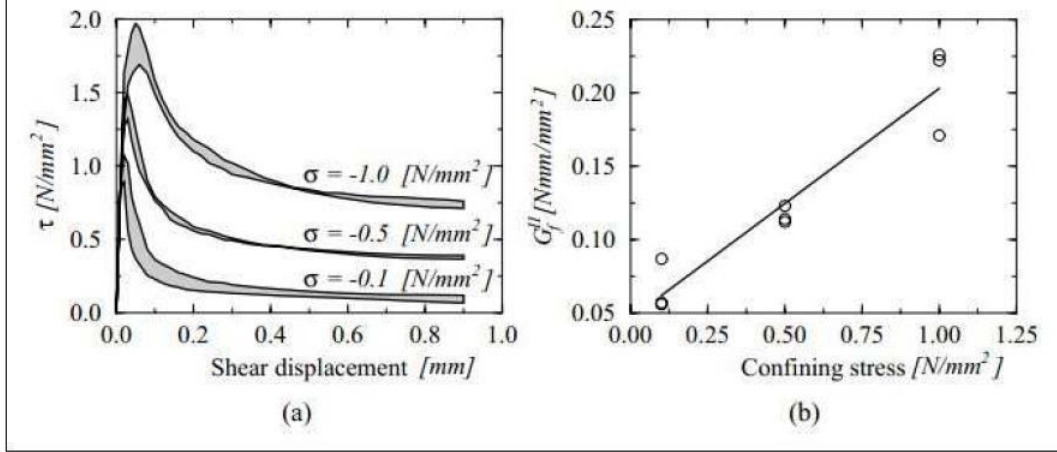


Figure 3.6: Typical shear bond behaviour of the joints for solid clay units, Pluijm [14]: (a) stress-displacement diagram for different normal stress levels; (b) mode II fracture energy G_f^{II} as a function of the normal stress level.

Pluijm [14] presents the most complete characterization of the masonry shear behaviour for solid clay and calcium-silicate units. This involves a direct shear test under different levels of uniform state of stress. This test did not allow for application of tensile stresses and low confining stresses. Because it results in extremely brittle failure, which makes the test set-up potential installable. Where as, for higher confining stresses shearing of the unit-mortar interface is accompanied by diagonal cracking in the units.

These experimental results yield an exponential shear softening with a residual dry friction, see Figure 3.6(a). The area defined by the stress-displacement diagram and the residual dry friction shear level is called mode II fracture energy G_f^{II} . The value for the fracture energy depends also on the level of the confining stress, see Figure 3.6(b). Evaluation of the net bond surface of the specimens is no longer possible in this case.

Moreover, it has been found that behaviour of masonry is no longer associative i.e. $\delta_{nn} \neq \delta_{tt} \tan \phi$ (δ_{nn} and δ_{tt} is normal and tangential relative displacement). Thus an additional material parameters can be obtained from such an experiment i.e. dilatancy angle, see Figure 3.7. The dilatancy angle ψ measures the uplift of one unit over the other upon shearing. It depends on the level of the confining stress, see Figure [4.6], i.e. for high confining pressures ψ decreases to zero. Further more, dilatancy also decreases with increasing in shear displacement, due to the smoothing of the sheared surfaces.

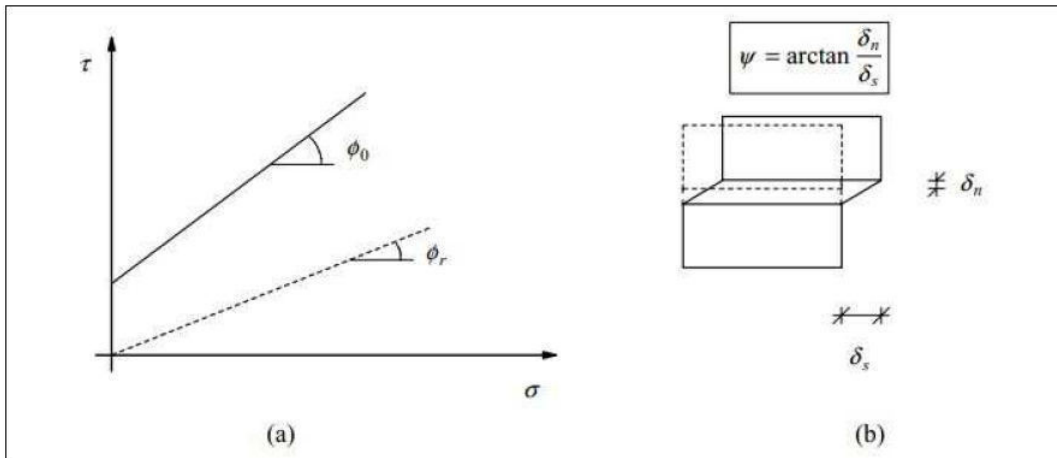


Figure 3.7: Definition of friction and dilatancy angles lourenco1996[1]: (a) Coulomb friction law, with initial and residual friction angle; (b) dilatancy angle as the uplift of neighbouring units upon shearing.

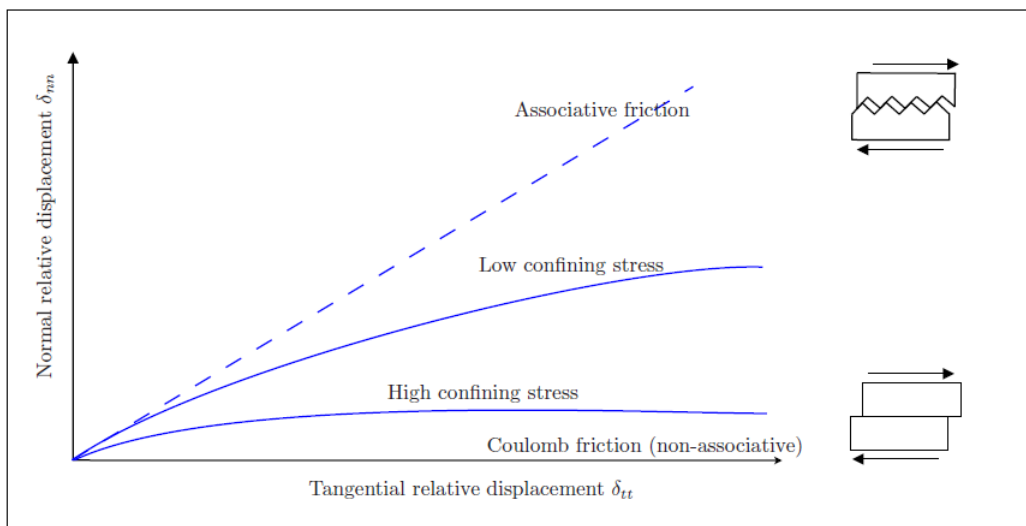


Figure 3.8: Masonry joint behaviour: relation between normal and tangential relative displacement for different confining stress.

Chapter 4

Modelling Strategies of Masonry

4.1 Different modelling strategies for masonry

4.1.1 Modelling with FEM

The presence of vertical and horizontal mortar joints causes the masonry to be anisotropic. Basically, the following different approaches have been adopted to model such anisotropy:

1. Micro model The discretization follows the actual geometry of both the blocks and mortar joints, adopting different constitutive models for the two components. Particular attention must be paid in the modelling of joints, since the sliding at joint level often starts up the crack propagation. Although this approach may appear very straightforward, its major disadvantage comes from the extremely large number of elements to be generated as the structure increases in size and complexity. This renders unlikely the use of micro models for the global analysis of entire buildings, also considering the fact that the actual distribution of blocks and joints might be impossible to detect unless invasive investigations are performed

2. Macro model The macro model assumes that the masonry structure is a homogeneous continuum to be discretized with a finite element mesh which does not copy the wall organism, but obeys the method's own criteria. The single element will thus have a constitutive model which must be capable of reproducing an average behaviour. This assumption bypasses the physical characteristics of the problem. Nevertheless the equivalent material models have proven to be able to grasp certain aspects of the global behaviour without the number of parameters and the computing effort needed is reduced

3. Homogenization

On-going to macro-modelling, continuum parameters must be assessed by experiments on specimens of sufficiently large size, under homogeneous states of stress or strain (Dhanasekhar *et al.*) [18,19] As an alternative to difficult experimental tests, it is possible to assess experimentally the individual components (or simple wallets and cores, see Benedetti *et al.* [17]. This obtained data for individual components are considered as input parameters for the numerical homogenization technique.

The homogenization theory allows the global behaviour (macro-constitutive) to be derived from the behaviour of its constitutive materials or micro-constitutive laws (Anthoine [24], Luciano and Sacco [25]; Gambarotta and Lagomarsino [22,23] Zucchini and Lourenco [20]. Such methodologies requires to identifying a basic cell, which generates an entire panel by its regular repetition, see

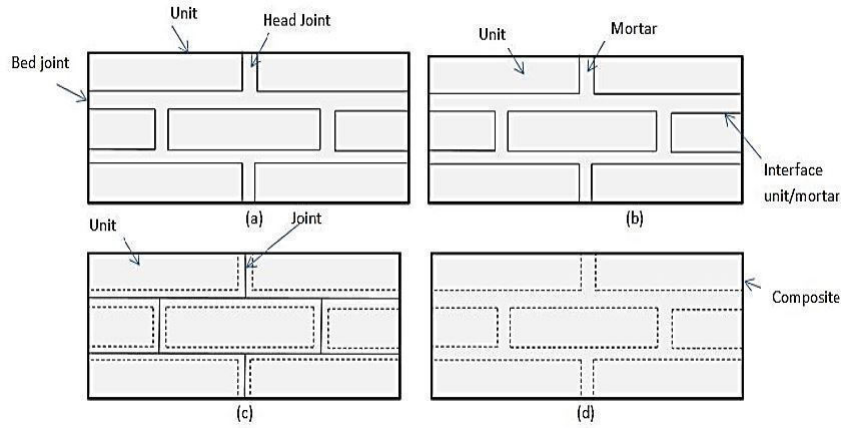


Figure 4.1: Modelling of masonry structures (a) masonry sample; (b) detailed micro modelling; (c) simplified micro-modelling; (d) macro modelling

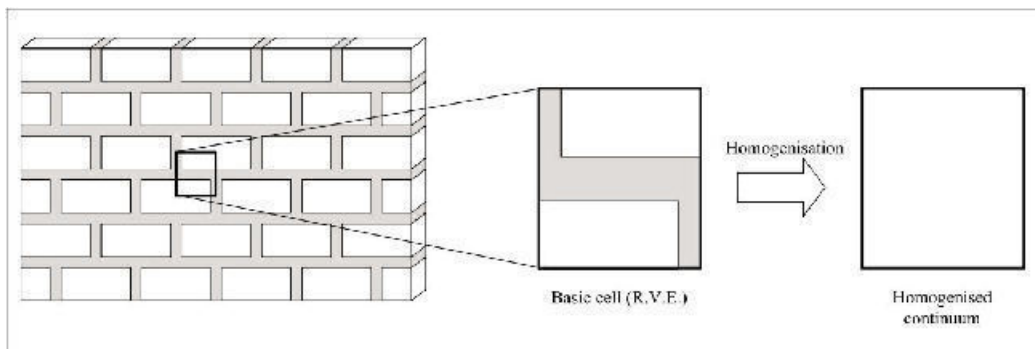


Figure 4.2: Basic cell for masonry and objective of homogenisation [20]

Figure 4.2. In this way by exploiting periodicity of the masonry average macro-constitutive law can be obtained from a single basic unit cell. Initially, the homogenization technique had been performed in several successive steps, head joints and bed joints were being introduced successively. In later work homogenization theory for periodic media is rigorously applied to the basic cell to carry out a single step homogenization, with adequate boundary conditions and exact geometry. Finite element method was used to obtain numerical solution as exact solutions is not possible[24,26].

Zucchini and Lourenco [20] proposed an improved micro-mechanical homogenization model for masonry analysis in non-linear domain. The model was coupled with damage and plasticity models, by suitably chosen deformation mechanisms. Moreover, the model was capable of simulating the behaviour of a basic periodic cell up to complete degradation and failure, see Figure ??.

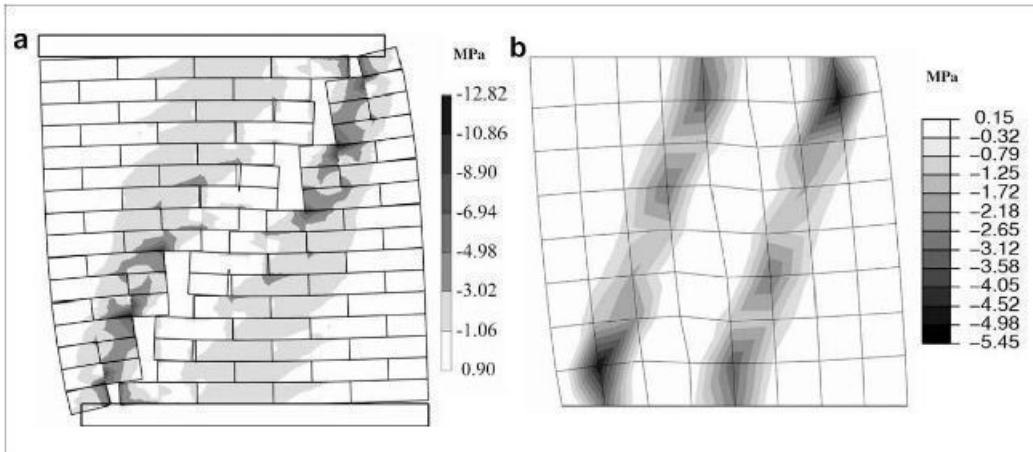


Figure 4.3: Minimum principal stresses for test: (a) interface model at $d = 4.1$ mm; (b) homogenisation model coupled with damage and plasticity at $d = 3.1$ mm [21].

20]

4.2 Modelling with interface elements

In this approach, the blocks are modelled using conventional continuum elements, linear or non-linear, while mortar joints are simulated by interface elements, the ‘joint elements’, made up of two rows of superimposed nodes, with friction constitutive law. The introduction of the joint is easy to implement in a software programme, since the nodal unknowns are the same for continuum and joint elements, though for the latter the stress tensor must be expressed in terms of nodal displacements instead of deformation components. Two major concerns balance the apparent simplicity of this approach [27] Block mesh and joint mesh must be connected together, so that they have to be compatible, which is possible only if interface joints are identically located. This compatibility is very difficult to ensure when complex block arrangements are to be handled, like in 3D structures. and The joint element is intrinsically able to model the contact only in the small displacement field. When large motion are to be dealt, is not possible to provide easy remeshing in order to update existing contacts and/or to create new ones [12].

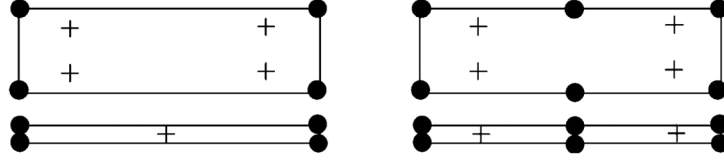


Figure 4.4: Degeneration of continuum element into ‘joint’ element

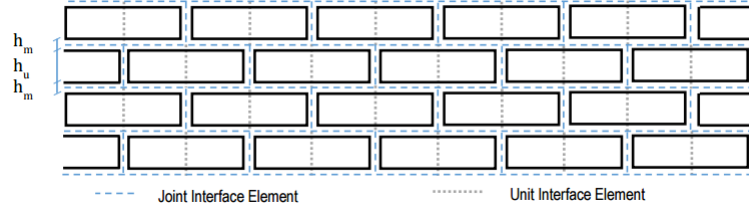


Figure 4.5: Modelling Strategy for Masonry adopted.

4.3 Modelling with DEM

The above-mentioned limitations are overcome by the DEM. In this approach, the structure is considered as an assembly of distinct blocks, rigid or deformable, interacting through unilateral elasto-plastic contact elements which follow a Coulomb slip criterion for simulating contact forces. The method is based on a formulation in large displacement (for the joints) and small deformations (for the blocks), and can correctly simulate collapse mechanisms due to sliding, rotations and impact. The contacts are not fixed, like in the FEMDE, so that during the analyses blocks can lose existing contacts and make new ones. Once every single block has been modelled both geometrically and mechanically, and the volume and surface forces are known, the time history of the block’s displacements is determined by explicitly solving the differential equations of motion. The main advantage of this approach is the possibility of following the displacements and determining the collapse mechanism of structures made up of virtually any number of blocks [28,29]. On the contrary it must be considered that the finite elements used for the internal mesh of the blocks, when deformable, show poor performance, so the method is not accurate for the study of stress states within the blocks[12]. For this purpose, other models are more suitable. However, this method is not discussed in this thesis.

Micro-models is best tool to understand the behaviour of masonry. This requires the consideration of the failure mechanisms of the masonry and its constituent. These failure mechanisms are lumped into a interface element, with the assumption that all the inelastic behaviour occurs in interface element which leads to robust type of modelling, capable to tracing complete load path(as in figure. The interface element shows the failure mechanism as potential crack, slip and crushing.

4.4 Material and structural behavior of masonry

A unique model is not realistic because masonry structures differ in materials, texture and structural details. Analysts should choose the model that best suited his case, taking into account the infor-

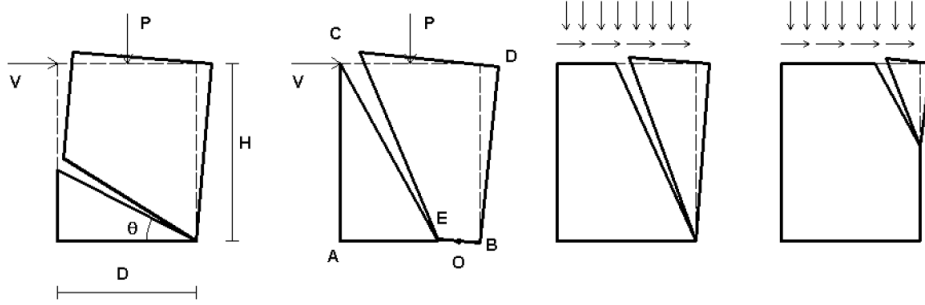


Figure 4.6: Possible failure mechanism in masonry panels (adapted from [11])

mation searched (serviceability, damage, collapse), the accuracy required (local or global behavior), the input data needed (information about material) and finally, costs (that include, also the time needed to complete the analysis).

4.4.1 Limit analysis

The simplest method used to describe masonry comes from the Mechanics of Solids and allows the study of the kinetics of collapse through the limit equilibrium analysis.

With the basic assumptions of the method (which include no tensile strength and infinite compressive strength), the masonry panel can be modelled as kinematic chain of rigid blocks, described with the Lagrangian displacement magnitude at one point. Once suggested the failure mechanism, the system is reduced to an equivalent single degree of freedom (SDF) system where the horizontal static load factor can be calculated at the threshold of the system. With the assumption of rigid behavior until the establishment of linkage, the load factor represents the value (in g) of the horizontal acceleration at failure, associated to the mechanism suggested. The failure mechanisms can be divided into two types [11]. The mechanisms of first type relate to the out-of-plane behavior of masonry (out of plane bending and rocking.), while the mechanisms of second type include the in-plane behavior of the panel (shear and bending damage). With the aforementioned limit analysis method, the first failure mechanism is studied in an acceptable way, however, the second failure mechanism is assessed in an excessively precautionary way.

Disadvantages of the method just described are that it does not take into account the elastic deformation of the structure and the post-elastic behavior; infact the strategy always leads to the study of equilibrium and kinematics of rigid bodies. Nevertheless, in the case of complex kinematics, the method has been very useful for evaluating the effects of consolidations. An important application of the limit principles is the analysis of masonry arch [11]. Heyman's idea was that as most voussoir arches have low stresses and lines of thrust lie well within the masonry which mean that factors of safety have little relevance, thus a geometrical factor of safety may be defined. The geometrical factor considers the minimum thickness arch of the same shape as the real arch, which would just contain a proper line of thrust. This kind of analysis was applied to the stone arch between the western towers of Lincoln Cathedral and the Ponte Mosca in Turin and shows that the effect of geometry changes due to yielding of the abutments

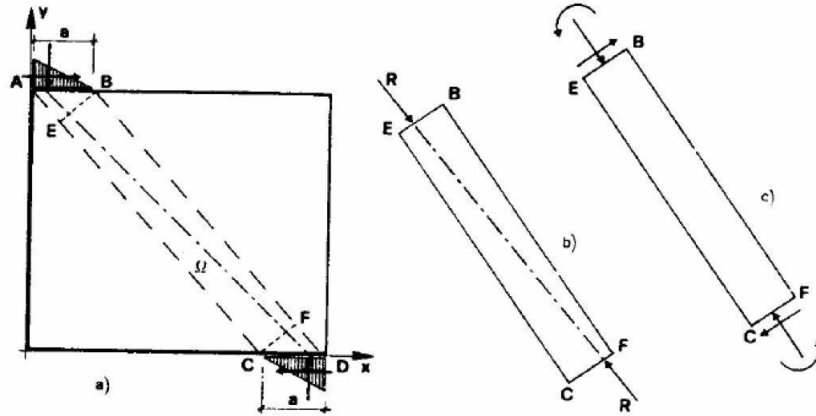


Figure 4.7: Masonry panel modelled through an equivalent strut

4.4.2 Equivalent strut

Another possibility for modelling masonry is the equivalent strut approach, which consider deformations in the elastic range possibly followed by inelastic deformation. Models which belong to this class may be bi-dimensional or mono dimensional.

Bi-dimensional approaches see masonry panels as equivalent elements with two main dimensions, while in a mono-dimensional approach, the masonry panel is divided into piers and lintels, regarded as equivalent struts. The connecting rod (strut) corresponds to the reactive part of the masonry panel, thus its inclination and its stiffness must reproduce the average behavior of the wall. Each panel can be in crisis if the equilibrium is not respected or cracks occur

4.4.3 Macro-elements: equivalent models and frame models title

With the approach of macro-elements, masonry panels are represent as a combination of structural elements (piers and lintels) as shown in figure 2.4. The macro-elements approach needs low computational efforts because of the reduction of the degrees of freedom, but this method gives a rough description of the masonry elements. Usually, analysts choose the macro-elements approach when the object of the analysis is the global behavior of an entire structure (under cyclic loading). An example of macro-element is the model proposed by Gambarotta and Lagomarsino [7]. Their approach (which was able to catch both overturning and hysteretic mechanism) has two degrees of freedom and was especially for rectangular masonry panels. Their work was then improved [1], and a non linear macro-element model was proposed. Figure shows the macro-element; the structure is divided into three sub-structures. There are two layers (inferior and superior) where bending and axial effects are concentrate, while shear deformation are presented only in the central part.

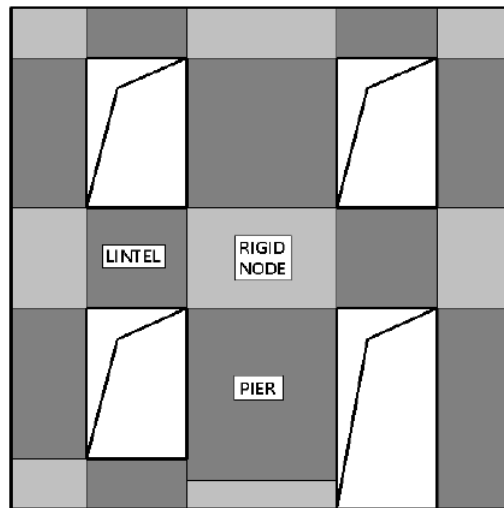


Figure 4.8: An example of macro-element modeling of a masonry wall

Chapter 5

The Constitutive Model for Cyclic loading

5.1 The Constitutive Model for Cyclic loading

Cyclic behavior of interface can be reproduced by adopting relevant non linear Constitutive material laws .This model is fully based on an incremental formulation of plasticity theory and derives from an existing constitutive model developed for a Monotonic loading The development of constitutive models for the analysis of structures submitted to cyclic loading should consider the main relevant features that characterize cyclic behaviour.[33] Recent experimental work from Literature(for instance see[29 -32]) carried out to investigate cyclic behaviour of interfaces has shown some important characteristics, summarized as

- Stiffness degradation in both tension and compression regimes
- Residual relative normal displacements at zero stress
- Absence of stiffness degradation in direct shear
- Complete crack closing under compressive loading

Accordingly, Non-linear constitutive material laws should be adopted for tensile and compressive loading and elastic behaviour constitutes a satisfactory approach for shear unloading/reloading behaviour

5.1.1 Elastic behaviour

A constitutive model establishes a relation between generalized stress and strain vectors, usually expressed as

$$\boldsymbol{\sigma} = \mathbf{K}\boldsymbol{\epsilon} \quad (5.1)$$

where \mathbf{K} represents the stiffness matrix

The above constitutive equations depicts the relationship between the traction vector and the relative displacement vector along the zero-thickness line interface elements For a 2D case, $\boldsymbol{\sigma} = \{\sigma_{nn}, \sigma_{tt}\}^T$, $\boldsymbol{\epsilon} = \{\epsilon_{nn}, \epsilon_{tt}\}^T$ and $\mathbf{K} = \text{diag}\{k_{nn}, k_{tt}\}^T$ where nn and tt designate normal and tangential components

The component of elastic stiffness matrix \mathbf{K} can be written as

$$\frac{1}{k_{nn}} = \frac{1}{h_m} \left(\frac{1}{E_b} + \frac{1}{E_m} \right) \quad (5.2)$$

$$\frac{1}{k_{tt}} = \frac{1}{h_m} \left(\frac{1}{G_b} + \frac{1}{G_m} \right) \quad (5.3)$$

Where E_b , E_m , G_b and G_m are the elastic Young's moduli and the elastic shear moduli for brick unit and mortar. h_m is the actual thickness of mortar joint.

5.1.2 Plastic behaviour

In the present study a rate independent composite interface model, defined by hyperbolic function has been used to develop a Cyclic Model . The proposed Cyclic model is a simple extension of the Monotonic Model having Mohr-Coulomb criteria with cut-off in tension and cap-off in compression[34] , which result in the single surface yield criteria capable of representing pressure-dependent friction shear failure and cracking by cut-off in-tension and crushing by cap-off in compression under combined normal and tangential stresses. The model includes all the mechanisms of the masonry failure and also overcomes the problem of the singularity that occurs in multi-surfaces yield criteria. In order to include unloading/Reloading Behaviour an extension of Plasticity theory is proposed by introducing two new Yield Surfaces in Unloading to tension and Compression in a monotonic model [33]

5.1.3 Unloading or Reloading to tension

Unloading/reloading to tension can be started from any allowable stress point, except from points on the monotonic tensile cut off and ruled according to the yield function

$$F(\boldsymbol{\sigma}, \mathbf{q}_{ut}, \mathbf{a}, \kappa_{ut}) := -[(C - \tilde{\sigma}_{nn} \tan(\phi))]^2 f_c(\boldsymbol{\sigma}, \mathbf{q}_{ut}, \mathbf{a}) f_t(\boldsymbol{\sigma}, \mathbf{q}_{ut}, \mathbf{a}) + \tilde{\sigma}_{tt}^2 \quad (5.4)$$

$$f_t(\boldsymbol{\sigma}, \mathbf{a}, \mathbf{q}_{ut}) := \frac{2}{\pi} \arctan \left(\frac{\xi - \tilde{\sigma}_{nn}}{\alpha_t} \right) \quad (5.5)$$

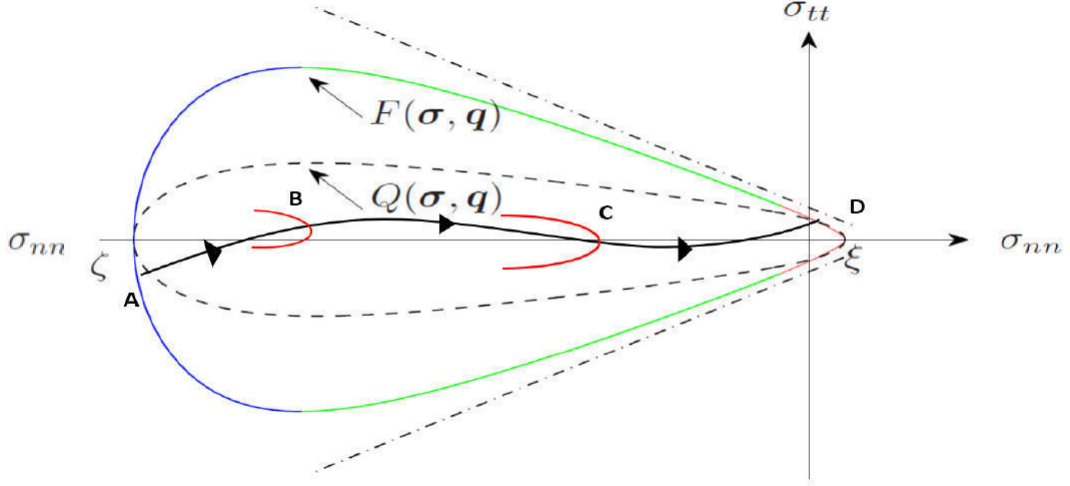


Figure 5.1: Hypothetical Motion of Unloading Yield surface in stress space to Tension(from A to D)

where q_{ut} is the tensile unloading hardening parameter.

Relative or Reduced stress

The relative (or reduced) stress vector $\tilde{\sigma}$ is given by $\tilde{\sigma} = \sigma - \mathbf{a}$

5.1.4 Unloading or Reloading to Compression

unloading/reloading to compression can take place from any acceptable stress point, except from points on the monotonic compressive surface being controlled by the following yield function and compression cap f_c

$$F(\sigma, \mathbf{q}_{uc}, \mathbf{a}, \kappa_{uc}) := -[(C - \tilde{\sigma}_{nn} \tan(\phi))]^2 f_c(\sigma, \mathbf{q}_{uc}, \mathbf{a}) f_t(\sigma, \mathbf{q}_{uc}, \mathbf{a}) + \tilde{\sigma}_{tt}^2 \quad (5.6)$$

$$f_c(\sigma, \mathbf{a}, \mathbf{q}_{uc}) := \frac{2}{\pi} \arctan\left(\frac{\tilde{\sigma}_{nn} - \zeta}{\alpha_c}\right) \quad (5.7)$$

where q_{uc} is the Compressive unloading hardening parameter.

Where the vector $\mathbf{q} = \mathbf{q}(C, C_q, \phi, \psi, \xi, \zeta)$ is a function of six internal hardening parameters, which implicate the apparent cohesion (C, C_q), friction angle (ϕ), dilation angle (ψ), tensile strength (ξ) and compression strength (ζ). In the yield function, ξ denotes tension cut-off and ζ denotes compression cap. The function $f_c(\sigma, \mathbf{q})$ and $f_t(\sigma, \mathbf{q})$ are the compression cap and tension cut-off functions respectively. The function $f_c(\sigma, \mathbf{q})$ has the zero value at the cap and the function $f_t(\sigma, \mathbf{q})$ has zero value at tension-cut. For all other stress-states both the function have value approximately

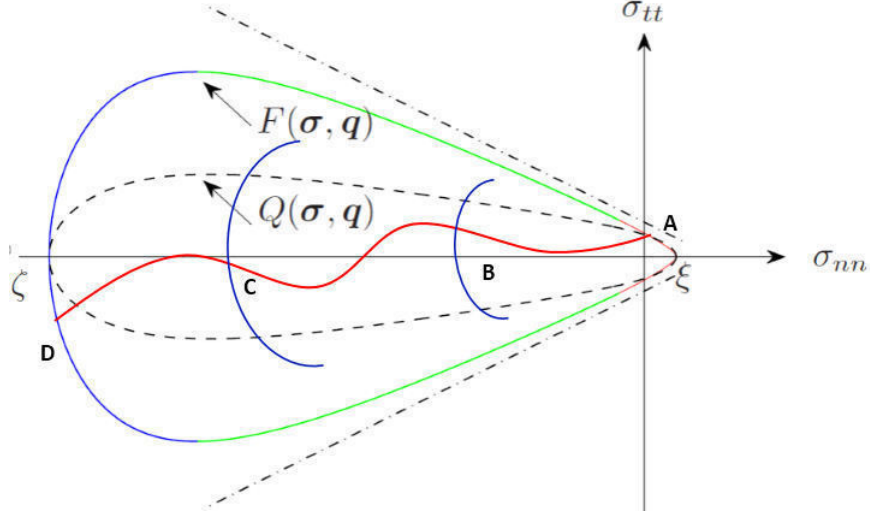


Figure 5.2: Hypothetical Motion of Unloading Yield surface in stress space to compression (from A to D)

equal to one. The parameters α_c and α_t control the curvature of the compression cap and tension cut-off at transition region.

A non-associated formulation is used because friction and dilatency angles are considerably different as mentioned by van2000, atkinson1989. Therefore, the plastic potential is described in terms of another hyperbolic function with different values of apparent cohesion (C_q) and frictional angle (dilation angle (ψ)), with same tensile (ξ) and compressive strength (ζ). The expression of potential function reads

$$Q(\boldsymbol{\sigma}, \mathbf{q}, \mathbf{a}) := -[C_q - \tilde{\sigma}_{nn} \tan(\psi)]^2 f_c(\boldsymbol{\sigma}, \mathbf{q}, \mathbf{a}) f_t(\boldsymbol{\sigma}, \mathbf{q}, \mathbf{a}) + \tilde{\sigma}_{tt}^2 \quad (5.8)$$

5.1.5 Mixed Hardening Law

Unloading surfaces are ruled by mixed hardening laws, for which a definition of the back-stress vector \mathbf{a} is defined, The evolution of the back stress vector is assumed to be given by

$$\dot{\mathbf{a}} = (1 - M) \lambda_u K_{ks} \mathbf{u}_a$$

where K_t = kinematic Secant hardening modulus which is a function of Unloading hardening parameter and the Kinematic effective stress

λ_u is the unloading plastic multiplier rate and

\mathbf{u}_a is the unitary vector of \mathbf{a}

The scalar M provides the proportion of isotropic and kinematic hardening $0 \leq M \leq 1$

5.1.6 Evolution laws

Evolution laws for hardening or softening behaviour for the composite interface model is defined by the rate of plastic work per unit of volume. During plastic loading internal variables can be express as

$$\dot{\mathbf{W}}^p := \tilde{\boldsymbol{\sigma}}^T \boldsymbol{\epsilon}^p \quad (5.9)$$

Where $\dot{\mathbf{W}}^p$ is the rate of plastic work hardening per unit of volume. In the present study, evolution of yield surface in tension-shear and compression-shear region has been assumed such that during plastic loading in tension-shear region, tensile strength (ξ) decreases exponentially while friction angle (ϕ) remain unchanged, and in compression-shear region both friction and tensile strength both degrades exponentially. In addition, the compression strength changes when plastic loading path intersects with the compression cap. The above assumptions can be expressed by four internal variables i.e. $\dot{\mathbf{W}}^p := \dot{\mathbf{W}}^p(w_1^p, w_2^p, w_3^p, w_4^p)$ where \dot{w}_1^p and \dot{w}_2^p represent degradation in tensile strength, \dot{w}_2^p and \dot{w}_3^p govern the frictional strength degradation and \dot{w}_4^p gives change in the compression strength.

$$\dot{w}_1^p := \langle \tilde{\sigma}_{nn} \rangle \dot{u}_{nn}^p \quad (5.10)$$

$$\dot{w}_2^p := (\tilde{\sigma}_{tt} - \tilde{\sigma}_{tt,r1} \text{sign}(\tilde{\sigma}_{tt})) \dot{u}_{tt}^p \quad (5.11)$$

$$\dot{w}_3^p := (\tilde{\sigma}_{tt,r1} - \tilde{\sigma}_{tt,r2}) \text{sign}(\tilde{\sigma}_{tt}) \dot{u}_{tt}^p \quad (5.12)$$

$$\dot{w}_4^p := \langle \langle \tilde{\sigma}_{nn} \rangle \rangle \dot{u}_{nn}^p \quad \text{for } \tilde{\sigma}_{nn} < \zeta_c \quad (5.13)$$

Where the symbol $\langle \rangle$ denotes for Macaulay bracket and $\langle x \rangle = (x + |x|)/2$ and $\langle \langle x \rangle \rangle = (x - |x|)/2$. ζ_c denotes the transient point from compression cap to Mohr-Coulomb friction envelope. $\tilde{\sigma}_{tt,r1}$ is the tangential strength when tensile strength is completely exhausted; $\tilde{\sigma}_{tt,r2}$ is minimum tangential strength for the final contracted yield surface. In tension-shear region, $\tilde{\sigma}_{tt,r1}$ and $\tilde{\sigma}_{tt,r2}$ are assumed to be zero and in compression-shear region they can be express as

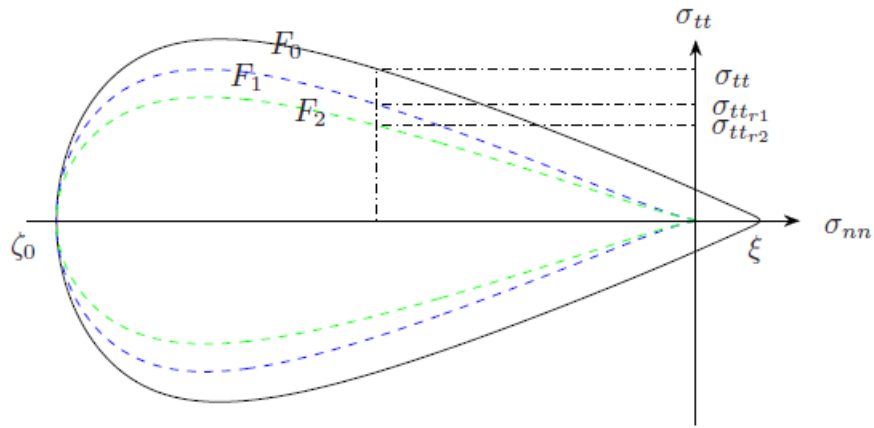
$$\tilde{\sigma}_{tt,r1}^2 = -2C_r \tan \phi f_c f_t \quad (5.14)$$

$$\tilde{\sigma}_{tt,r2}^2 = -2C_r \tan \psi_r f_c f_t \quad (5.15)$$

In tension-shear region, during plastic loading the yield surface will contract until the tensile strength is exhausted and cohesion reaches a minimum value, i.e. yield surface contracts from F_0 to F_1 . While in compression-shear region, plastic loading reduces the tensile strength, cohesion as well as friction angle to its residual value (i.e. yield surface contracts to F_2). If the plastic loading path intersects the compression cap region, yield surface will evolve due to hardening in compression, i.e. yield surface evolves from F_0 to F_1 . After the compression-strength reaches its maximum value, there is a subsequent softening and compression strength reduces to minimum value due to contraction of yield surface i.e. yield surface contracts from F_1 to F_2 .

The hardening parameter \mathbf{q} can be related to the internal variables as follows

$$C := C_r + (C_0 - C_r) \exp \left(-\beta_C \left(\frac{w_1^p}{G_f^I} + \frac{w_2^p}{G_f^{II}} \right) \right) \quad (5.16)$$



(a)

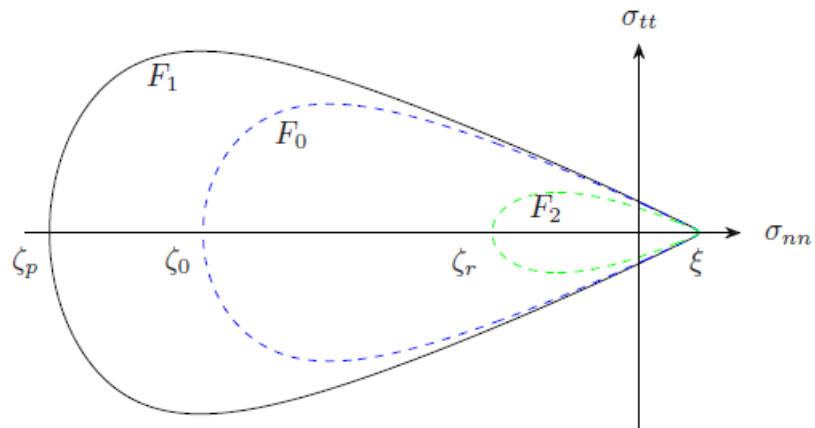


Figure 5.3:
(a) Evolution of Yield Surface in Compression and in Tension under Monotonic Loading

$$C := C_r + (C_0 - C_r) \exp^{-\beta_C \left(\frac{w_1^p}{G_f^I} + \frac{w_2^p}{G_f^{II}} \right)} \quad (5.17)$$

$$C_Q := C_{Q_r} + (C_{Q_0} - C_{Q_r}) \exp^{-\beta_{C_Q} \left(\frac{w_1^p}{G_f^I} + \frac{w_2^p}{G_f^{II}} \right)} \quad (5.18)$$

$$\phi := \phi_r + (\phi_0 - \phi_r) \exp^{-\beta_\phi w_3^p} \quad (5.19)$$

$$\psi := \psi_r + (\psi_0 - \psi_r) \exp^{-\beta_\psi w_3^p} \quad (5.20)$$

$$\xi := \xi_0 \exp^{-\beta_\xi \left(\frac{w_1^p}{G_f^I} + \frac{w_2^p}{G_f^{II}} \right)} \quad (5.21)$$

$$\zeta = \begin{cases} \zeta_0 + (\zeta_p - \zeta_0) \sqrt{\left(\frac{2w_4^p}{w_p} \right) - \left(\frac{w_4^p}{w_p} \right)^2} & \text{if } w_4^p \leq w_p \\ \zeta_0 + (\zeta_p - \zeta_0) \left(\frac{w_4^p - w_p}{w_m - w_p} \right)^2 & \text{if } w_p \leq w_4^p \leq w_m \\ \zeta_r + (\zeta_m - \zeta_r) \exp^{\beta_\zeta \left(\frac{w_4^p - w_p}{\zeta_m - \zeta_r} \right)} & \text{if } w_4^p > w_m \end{cases} \quad (5.22)$$

Where G_f^I and G_f^{II} are the mode I and mode II fracture energy and β_i is a parameter that controls the softening of the internal variable. The subscript 0 stands for initial value and r for residual value whereas subscript p and m indicate intermediate values. The preceding hardening equation can be written in a compact form as follows

$$\dot{W}^p = H \dot{\epsilon}^p \quad (5.23)$$

5.1.7 Unloading Yield Surfaces

Two new auxiliary yield surfaces (termed unloading surfaces) similar to the monotonic ones were introduced in the monotonic model, so that unloading to tension and to compression could be modelled.

5.1.8 Characteristics of unloading surfaces

- Each unloading surface moves inside the admissible stress space towards the similar monotonic yield surface.
- In a given unloading process, when the stress point reaches the monotonic yield surface, the surface used for unloading becomes inactive and the loading process becomes controlled by the

monotonic yield surface

- If a stress reversal occurs during an unloading process, a new unloading surface is started, subsequently deactivated when it reaches the monotonic envelope

5.1.9 Possible Cyclic loading movements of the Constitutive Model

Two unloading cases from the monotonic envelope are considered which can be further classified into three cases each

- 1.unloading to tension (CT)
- 2.unloading to compression (TC).

In above both cases, a stress reversal can occur even before the monotonic envelope has been reached, leading to following movements

- 3.Reloaded movements to compression (CTC)
- 4.Reloaded movements to Tension (TCT)

Two new cases may originate if a reversal situation happens before stresses reach the monotonic envelope.They are

- 5.Reversal Case (CTCT)
- 6.Reversal Case (TCTC)

5.1.10 Hardening laws adopted for unloading Cases

A curve that relates the unloading hardening parameter κ_u and the unloading effective stress σ_u must be defined.

$$\begin{aligned}\dot{\kappa}_{ut} &= |\dot{u}_n^p| = \dot{\lambda}_{ut} \\ \dot{\kappa}_{uc} &= \dot{\lambda}_{uc}\end{aligned}$$

5.1.11 Evolution of hardening parameters

Curves that relates the unloading hardening parameter q_u and the unloading effective stress σ_u must be defined

The complete definition of the hardening laws requires the need of four additional material parameters with respect to the monotonic version, which can be obtained from uni axial cyclic experiments under tensile and compressive loading

The Evolution of Hardening Parameters are based on the curves developed from the special points mentioned in figure [2]

Table 5.1: Experimental parameters adopted

Numerical simulation	κ_1/κ_t	κ_1/κ_c	κ_2/κ_c	$\Delta_{\kappa_c}/\kappa_t$
Gopalaratnam and Shah(1985)	0.76	-	-	-
Karsan and Jirsa	-	0.56	0.28	0.13
Reinhardt(1984)	0.73	-	-	-

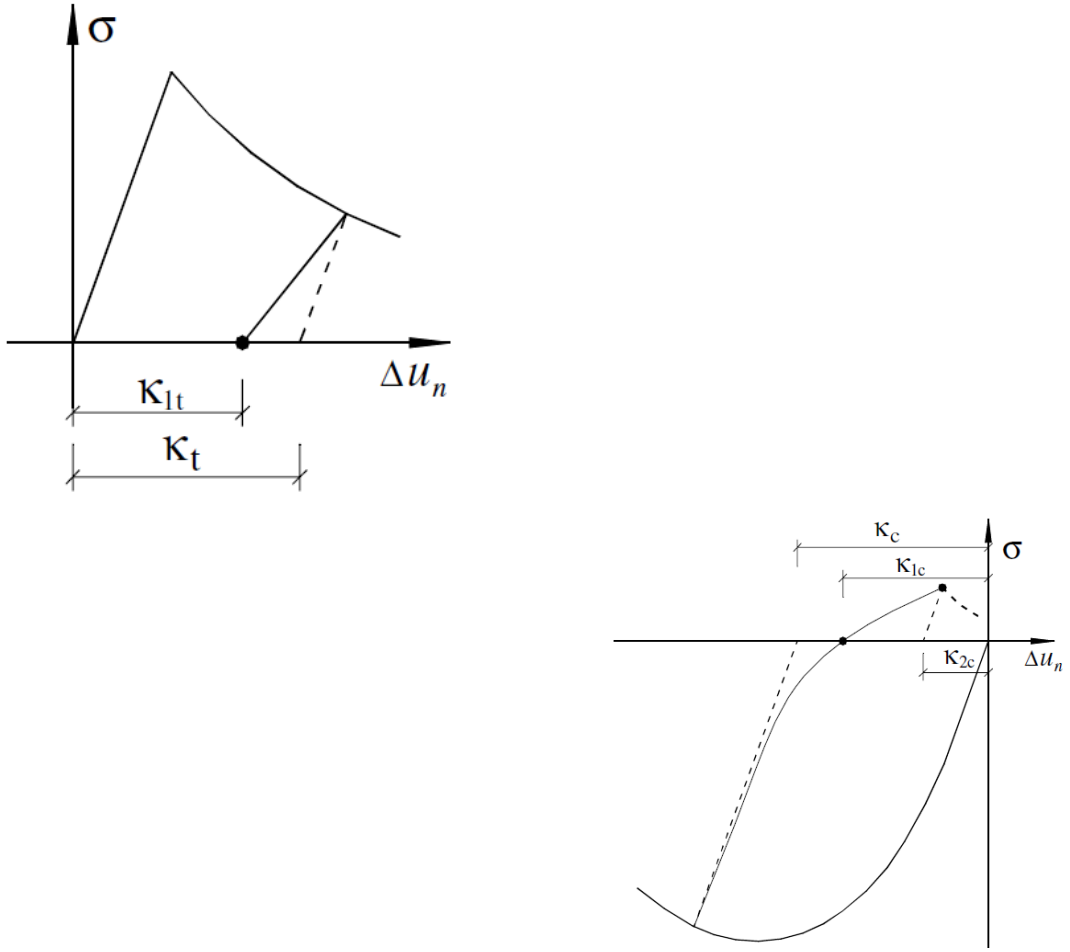


Figure 5.4: Special points at the uniaxial stress and displacement curves in compressive and tensile loading

5.1.12 Elastic-plastic tangent modulus

The total strain ϵ can be decomposed into sum of elastic strain and plastic strain i.e.

$$\epsilon = \epsilon^e + \epsilon^p \quad (5.24)$$

Where ϵ^e and ϵ^p are the elastic strain and plastic strain or irreversible strain respectively and the notion of irreversibility of plastic flow can be introduced by non-associated flow rule. It can be written in rate form as

$$\dot{\epsilon}^p = \dot{\lambda}_u \mathbf{m} \quad (5.25)$$

Where $\dot{\lambda}$ is the unloading constant slip rate or plastic multiplier. The plastic multiplier can be found by checking the consistency condition (persistence condition) together with Kuhn-Tucker condition ($F \leq 0, \dot{\lambda} \geq 0, \dot{\lambda} F = 0$). The consistency condition can be written as $\dot{\lambda} \dot{F} = 0$ for yield condition $\dot{\lambda} > 0$ and $\dot{F} = 0$ and we can be written it as

$$\dot{F} = \frac{\partial F}{\partial \boldsymbol{\sigma}} \dot{\boldsymbol{\sigma}} + \frac{\partial F}{\partial \mathbf{q}} \dot{\mathbf{q}} + \frac{\partial F}{\partial \mathbf{a}} \dot{\mathbf{a}} = 0 \quad (5.26)$$

$$\mathbf{n} : \mathbf{K} : \boldsymbol{\epsilon} - \mathbf{n} : \mathbf{K} : \dot{\lambda} \mathbf{m} - \mathbf{p} \dot{\lambda} \boldsymbol{\varpi}_u + (1 - M) \dot{\lambda} \mathbf{K}_{ks} u_a = 0 \quad (5.27)$$

$$\dot{\lambda} = \frac{\mathbf{n} \mathbf{K} \boldsymbol{\epsilon}}{\mathbf{n}^T \mathbf{K} \mathbf{m} + \mathbf{p}^T \boldsymbol{\varpi} + s(1 - M) \mathbf{K}_{ks} u_a} \quad (5.28)$$

In which $\mathbf{m} := \partial Q / \partial \boldsymbol{\sigma}$, $\mathbf{n} := \partial F / \partial \boldsymbol{\sigma}$, $s := \partial F / \partial \tilde{\mathbf{a}}$, $\mathbf{p} := \partial Q / \partial \lambda_u$, $\boldsymbol{\varpi}_u := (\partial q_u / \partial \mathbf{W}^p)(\partial \mathbf{W}^p / \partial \boldsymbol{\epsilon}^p)(\partial \boldsymbol{\epsilon}^p / \partial \lambda) = (\partial q_u / \partial W^p) H m$ and \mathbf{K}_{ks} is the Kinematic Secant hardening Modulus which is a function of the unloading Hardening parameter and the kinematic effective stress (Feenstra and De Borst, 1992). Now we can define hardening parameter in its rate form as $q_u = \dot{\lambda}_u \boldsymbol{\varpi}_u$. Putting the plastic multiplier ($\dot{\lambda}$) in the rate form of stress-strain relationship to get elasto-plastic tangent modulus K^{ep} , i.e.

$$\dot{\boldsymbol{\sigma}} = \mathbf{K}(\dot{\boldsymbol{\epsilon}} - \dot{\lambda} \mathbf{m}) = \mathbf{K}^{ep} \dot{\boldsymbol{\epsilon}} \quad (5.29)$$

$$\mathbf{K}^{ep} = \mathbf{K} - \frac{\mathbf{K} \mathbf{m} \otimes \mathbf{n} \mathbf{K}}{\mathbf{n}^T \mathbf{K} \mathbf{m} + \mathbf{p}^T \boldsymbol{\varpi} + s(1 - M) \mathbf{K}_{ks} u_a} \quad (5.30)$$

5.1.13 Algorithmic aspect of local and global solver

The Newton-Raphson scheme is used to solve non-linear system of equations, which leads to combined local and global approach.

Local solver provides the new internal state variable for a given relative displacement, subsequently global solver provides the solution for the unbalanced force to accommodate stress distribution within the finite load increments.

Elastic predictor-plastic correct strategy

The implicit backward Euler integration method is used to integrate the differential constitutive equations. For prescribed increment in strain $\dot{\boldsymbol{\epsilon}}$, at the next time step t_{n+1} i.e. $t_{n+1} = t_n + \Delta t$

The strain is given by $\boldsymbol{\epsilon}_{n+1} = \boldsymbol{\epsilon}_n + \Delta \boldsymbol{\epsilon}$,

This can be split into two part i.e.

$$\Delta \boldsymbol{\epsilon} = \Delta \boldsymbol{\epsilon}^e + \Delta \boldsymbol{\epsilon}^p.$$

According to the elastic predictor-plastic correct strategy, the stress and internal variables can be written in their incremental form as

$$\boldsymbol{\sigma}_{n+1} = \boldsymbol{\sigma}_n + \mathbf{K} \Delta \boldsymbol{\epsilon}^e = \boldsymbol{\sigma}_n + \mathbf{K}(\Delta \boldsymbol{\epsilon} - \Delta \boldsymbol{\epsilon}^p) \quad (5.31)$$

$$\boldsymbol{\sigma}_{n+1} = \boldsymbol{\sigma}_{n+1}^{trial} + \Delta \lambda_{n+1} \mathbf{K} \mathbf{m}_{n+1} \quad (5.32)$$

$$\mathbf{a}_{n+1} = \mathbf{a}_n + \Delta \lambda_{u,n+1} \mathbf{K}_{ks} u_{a,n+1} \quad (5.33)$$

$$\mathbf{q}_{u,n+1} = \mathbf{q}_{u,n} + \Delta \lambda_{u,n+1} \boldsymbol{\varpi}_{u,n+1} \quad (5.34)$$

$$\kappa_{u,n+1} = \kappa_{u,n} + \Delta_{u,n+1} \quad (5.35)$$

Where $\boldsymbol{\sigma}_{n+1}^{trial} = \boldsymbol{\sigma}_n + \mathbf{K} \Delta \boldsymbol{\epsilon}$ is the trial stress. During the elastic predictor step (say point A), if the trial stress goes outside the yield surfaces at the point B, see Figure) after cutting the yield surface at the contact point o ; $F(\boldsymbol{\sigma}_{n+1}^{trial}, \mathbf{q}_{n+1}) > 0$, then plastic corrector step projects the stress-state at the point D after the evolution or contraction of the yield surface due to the change in internal variable. In the Figure C represents the final converged stress-state for an elastic-perfectly plastic model. In the present study plastic step mobilizes the plastic work which changes the internal hardening parameter (\mathbf{q}) that expands or contracts the yield surface. It should be noted that the solution of the plastic corrector step must satisfy the full consistency at point D , rather than differential consistency ($\dot{F} = 0$).

$$F(\boldsymbol{\sigma}_{n+1}, \mathbf{q}_{n+1}, \mathbf{a}_{n+1}) = 0 \quad (5.36)$$

Contact point

The plastic corrector step only produces the change in the stress and internal variable ($\boldsymbol{\sigma}_n, \mathbf{q}_n$). Therefore, it is very important to find the contact point for the present elastic predictor step. Mathematically, it can be express as

$$F(\boldsymbol{\sigma}_n + \gamma \Delta \boldsymbol{\sigma}, \mathbf{q}_n, \mathbf{a}_n) = 0 \quad (5.37)$$

Where $\boldsymbol{\sigma}_n, \mathbf{q}_n$ are the variables from the last converged elastic or plastic step, and γ is unknown integer within the range $[0 \ 1]$, which converges the stress to the contact point.

Local iteration strategy

The backward Euler method gives rise to non-linear system of equations, which has to be solved to get actual stress state. In the present study full Newton-Raphson method is used to solve non-linear system of equations. It provides quadratic convergence with initial root sufficiently close, and also ensures the asymptotic quadratic convergence at the global level for structural equilibrium. Newton-Raphson strategy is used for the solution of non-linear equation in monolithic format, as illustrated in the Simo and Hughes for the J_2 plasticity. The strategy is highly influenced by the choice of the independent variables and sequence of the numerical operations. It requires the determination of residual for the set non-linear Equations . It can be written as

$$\mathbf{r}(\boldsymbol{\sigma}_{n+1}, \mathbf{q}_{n+1}, \mathbf{a}_{n+1}, \Delta \lambda_{u,n+1}) = \begin{cases} \boldsymbol{\sigma}_{n+1} - \boldsymbol{\sigma}_{n+1}^{trial} + \Delta \lambda_{u,n+1} \mathbf{K} \mathbf{m}_{n+1} = 0 \\ \mathbf{q}_{u,n+1} - \mathbf{q}_{u,n} + \Delta \lambda_{u,n+1} \boldsymbol{\varpi}_{u,n+1} = 0 \\ \mathbf{a}_{n+1} - \mathbf{a}_n - (1 - M) \Delta \lambda_{u,n+1} \mathbf{K}_{ks} \mathbf{u}_{a,n+1} = 0 \\ \kappa_{u,n+1} - \kappa_{u,n} - \Delta_{u,n+1} = 0 \\ F(\boldsymbol{\sigma}_{n+1}, \mathbf{q}_{u,n+1}, \mathbf{a}_{n+1}, \kappa_{n+1}, \Delta_{n+1}) = 0 \end{cases} \quad (5.38)$$

Linearization of the residual, and expanding the residual. we can write

$$\mathbf{r}(\boldsymbol{\sigma} + \delta\boldsymbol{\sigma}, \mathbf{q} + \delta\mathbf{q}, \mathbf{a} + \delta\mathbf{a}, \kappa_u + \delta\kappa_u, \Delta\lambda_u + \delta\lambda_u) = \mathbf{r}(\boldsymbol{\sigma}, \mathbf{q}, \mathbf{a}, \kappa_u, \Delta\lambda_u) + \frac{\mathbf{r}(\boldsymbol{\sigma}, \mathbf{q}, \mathbf{a}, \kappa_u, \Delta\lambda_u)}{\partial(\boldsymbol{\sigma}, \mathbf{q}, \mathbf{a}, \kappa_u, \lambda_u)} \begin{bmatrix} \delta\boldsymbol{\sigma} \\ \delta\mathbf{q} \\ \delta\mathbf{a} \\ \delta\kappa_u \\ \Delta\lambda_u \end{bmatrix} + O(\delta^2) \quad (5.39)$$

Where the truncation after first order term is zero ($O(\delta^2) \cong 0$) and $\frac{\mathbf{r}(\boldsymbol{\sigma}, \mathbf{q}, \mathbf{a}, \kappa_u, \Delta\lambda_u)}{\partial(\boldsymbol{\sigma}, \mathbf{q}, \mathbf{a}, \kappa_u, \lambda_u)}$ is the gradient of residual with respect to its dependent variable i.e. $\boldsymbol{\sigma}, \mathbf{q}, \mathbf{a}, \kappa_u, \lambda_u$ commonly known as Jacobian. The Jacobian for residual at time step n+1 can be express as

$$\mathbf{J}(\boldsymbol{\sigma}_{n+1}, \mathbf{q}_{n+1}, \mathbf{a}_{n+1}, \kappa_{u,n+1}, \Delta\lambda_{u,n+1})$$

The actual solution is achieved by letting the residual go to zero for that current time step during plastic loading. This can be achieved by performing iterations cycles. The iteration will end when residual will become smaller then prescribed

$$0 = \mathbf{r}(\boldsymbol{\sigma}_{n+1}^k, \mathbf{q}_{u,n+1}^k, \mathbf{a}_{n+1}^k, \kappa_{u,n+1}^k, \Delta\lambda_{u,n+1}^k) + \mathbf{J}^{-1}(\boldsymbol{\sigma}_{n+1}^k, \mathbf{q}_{u,n+1}^k, \mathbf{a}_{n+1}^k, \kappa_{u,n+1}^k, \Delta\lambda_{u,n+1}^k) \begin{bmatrix} \delta\boldsymbol{\sigma}_{n+1}^{k+1} \\ \delta\mathbf{q}_{u,n+1}^{k+1} \\ \delta\mathbf{a}_{n+1}^{k+1} \\ \delta\kappa_{u,n+1}^{k+1} \\ \Delta\lambda_{u,n+1}^{k+1} \end{bmatrix} \quad (5.40)$$

$$\begin{bmatrix} \delta\boldsymbol{\sigma}_{n+1}^{k+1} \\ \delta\mathbf{q}_{u,n+1}^{k+1} \\ \delta\mathbf{a}_{n+1}^{k+1} \\ \delta\kappa_{u,n+1}^{k+1} \\ \Delta\lambda_{u,n+1}^{k+1} \end{bmatrix} = -\mathbf{J}^{-1}(\boldsymbol{\sigma}_{n+1}^k, \mathbf{q}_{u,n+1}^k, \mathbf{a}_{n+1}^k, \kappa_{u,n+1}^k, \Delta\lambda_{u,n+1}^k) \mathbf{r}(\boldsymbol{\sigma}_{n+1}^k, \mathbf{a}_{n+1}^k, \mathbf{q}_{u,n+1}^k, \kappa_{u,n+1}^k, \Delta\lambda_{u,n+1}^k) \quad (5.41)$$

$$\begin{bmatrix} \boldsymbol{\sigma}_{n+1}^{k+1} \\ \mathbf{q}_{u,n+1}^{k+1} \\ \mathbf{a}_{n+1}^{k+1} \\ \kappa_{u,n+1}^{k+1} \\ \lambda_{u,n+1}^{k+1} \end{bmatrix} = \begin{bmatrix} \boldsymbol{\sigma}_{n+1}^k \\ \mathbf{q}_{u,n+1}^k \\ \mathbf{a}_{n+1}^k \\ \kappa_{u,n+1}^k \\ \lambda_{u,n+1}^k \end{bmatrix} + \begin{bmatrix} \delta\boldsymbol{\sigma}_{n+1}^{k+1} \\ \delta\mathbf{q}_{u,n+1}^{k+1} \\ \delta\mathbf{a}_{n+1}^{k+1} \\ \delta\kappa_{u,n+1}^{k+1} \\ \Delta\lambda_{u,n+1}^{k+1} \end{bmatrix} \quad (5.42)$$

Global iteration strategy

The converged solution form local iteration strategy can be used for the determination of consistent tangent operator $\frac{\Delta\boldsymbol{\sigma}}{\Delta\boldsymbol{\epsilon}}$ for the current time step. Thus, in order to compute the tangent operator using the Jacobian, we have to differentiate the residual with respect to the strain and then using the chain rule we will get

$$\frac{\partial}{\partial \epsilon} \begin{bmatrix} \boldsymbol{\sigma}_{n+1} - \boldsymbol{\sigma}_{n+1}^{trial} + \Delta \lambda_{u,n+1} \mathbf{K} \mathbf{m}_{n+1} \\ \mathbf{q}_{u,n+1} - \mathbf{q}_{u,n} + \Delta \lambda_{u,n+1} \boldsymbol{\varpi}_{u,n+1} \\ \mathbf{a}_{n+1} - \mathbf{a}_n - (1-M) \Delta \lambda_{u,n+1} \mathbf{K}_{ks} u_{a,n+1} \\ \kappa_{u,n+1} - \kappa_{u,n} - \Delta_{u,n+1} = 0 \\ F(\boldsymbol{\sigma}_{n+1}, \mathbf{q}_{u,n+1}, \mathbf{a}_{n+1}, \kappa_{n+1}, \Delta_{n+1}) = 0 \end{bmatrix} = 0 \quad (5.43)$$

$$\begin{bmatrix} \frac{\partial}{\partial \boldsymbol{\sigma}} & \frac{\partial}{\partial \mathbf{q}} & \frac{\partial}{\partial \mathbf{a}} & \frac{\partial}{\partial \kappa_u} & \frac{\partial}{\partial \lambda} \end{bmatrix}_{n+1} \begin{bmatrix} \boldsymbol{\sigma} + \Delta \lambda \mathbf{K} \mathbf{m} \\ q_u - \Delta \lambda \boldsymbol{\varpi} \\ a - (1-M) \Delta \lambda_u K_{ks} u_a \\ \kappa_u - \Delta_u \\ F(\boldsymbol{\sigma}, q, a, \kappa_u) \end{bmatrix}_{n+1} \begin{bmatrix} \frac{\partial \boldsymbol{\sigma}}{\partial \epsilon} & \frac{\partial \mathbf{q}_u}{\partial \epsilon} & \frac{\partial \mathbf{a}}{\partial \epsilon} & \frac{\partial \kappa_u}{\partial \epsilon} & \frac{\partial \lambda}{\partial \epsilon} \end{bmatrix}_{n+1}^T = \frac{\partial}{\partial \epsilon} \begin{bmatrix} \boldsymbol{\sigma} + \mathbf{K} \Delta \epsilon \\ q_u \\ a \\ \kappa \\ 0 \end{bmatrix}_n \quad (5.44)$$

$$\mathbf{J}(\boldsymbol{\sigma}_{n+1}, \mathbf{q}_{n+1}, \mathbf{a}_{n+1}, \kappa_{u,n+1}, \Delta \lambda_{u,n+1}) \cdot \begin{bmatrix} \frac{\partial \boldsymbol{\sigma}}{\partial \epsilon} & \frac{\partial \mathbf{q}_u}{\partial \epsilon} & \frac{\partial \mathbf{a}}{\partial \epsilon} & \frac{\partial \kappa_u}{\partial \epsilon} & \frac{\partial \lambda_u}{\partial \epsilon} \end{bmatrix}_{n+1}^T = \begin{bmatrix} \mathbf{K} \\ 0 \\ 0 \\ 0 \\ 0 \end{bmatrix} \quad (5.45)$$

$$\begin{bmatrix} \begin{bmatrix} \frac{\partial \boldsymbol{\sigma}}{\partial \epsilon} \\ \frac{\partial \mathbf{q}_u}{\partial \epsilon} \end{bmatrix}_{2 \times 2} \\ \begin{bmatrix} \frac{\partial \mathbf{a}}{\partial \epsilon} \\ \frac{\partial \kappa_u}{\partial \epsilon} \end{bmatrix}_{6 \times 2} \\ \begin{bmatrix} \frac{\partial \lambda}{\partial \epsilon} \end{bmatrix}_{2 \times 2} \\ \begin{bmatrix} \frac{\partial \lambda}{\partial \epsilon} \end{bmatrix}_{1 \times 2} \\ \begin{bmatrix} \frac{\partial \lambda}{\partial \epsilon} \end{bmatrix}_{1 \times 2} \end{bmatrix}_{12 \times 2} = J^{-1}(\boldsymbol{\sigma}_{n+1}, \mathbf{q}_{n+1}, \mathbf{a}_{n+1}, \kappa_{u,n+1}, \Delta \lambda_{n+1})_{12 \times 12} \begin{bmatrix} \mathbf{K} \\ 0 \\ 0 \\ 0 \\ 0 \end{bmatrix}_{12 \times 2} \quad (5.46)$$

The consistent tangent operator can be extracted from the preceding expression, and we can define the consistent tangent operator as:

$$\begin{bmatrix} \frac{\partial \boldsymbol{\sigma}}{\partial \epsilon} \end{bmatrix}_{2 \times 2} = O_{2 \times 2} \left\{ J^{-1}(\boldsymbol{\sigma}_{n+1}, \mathbf{q}_{u,n+1}, \mathbf{a}_{n+1}, \kappa_{u,n+1}, \Delta \lambda_{u,n+1})_{12 \times 12} \begin{bmatrix} \mathbf{K} \\ 0 \\ 0 \\ 0 \\ 0 \end{bmatrix}_{12 \times 2} \right\} \quad (5.47)$$

5.2 Appendix

Appendix

5.2.1 Yield Function

$$F(\boldsymbol{\sigma}, \mathbf{q}_u, \mathbf{a}, \kappa_u) = -[C - \tilde{\sigma}_{nn} \tan(\phi)]^2 f_c + [C - \xi \tan(\phi)]^2 f_c + \tilde{\sigma}_{tt}^2 \quad (5.48)$$

$$f_c(\boldsymbol{\sigma}, \mathbf{a}, \mathbf{q}_u) := \frac{2}{\pi} \arctan\left(\frac{\tilde{\sigma}_{nn} - \zeta}{\alpha}\right) \quad (5.49)$$

5.2.2 Potential Function

$$Q(\boldsymbol{\sigma}, \mathbf{q}_u, \mathbf{a}, \kappa_u) = -[C_Q - \tilde{\sigma}_{nn} \tan(\psi)]^2 f_c + [C_Q - \xi \tan(\psi)]^2 f_c + \tilde{\sigma}_{tt}^2 \quad (5.50)$$

5.2.3 Derivatives

$$T_1 = (C - \tilde{\sigma}_{nn} \tan(\phi)), T_2 = (C_Q - \tilde{\sigma}_{nn} \tan(\psi))$$

$$T_3 = (C - \xi \tan(\phi)), T_4 = (C_Q - \xi \tan(\psi))$$

$$D = 1 + (\tilde{\sigma} - \zeta/\beta)^2$$

$$\mathbf{n} = \frac{\partial F}{\partial \boldsymbol{\sigma}} \quad (5.51)$$

$$\mathbf{n} = \left[2T_1 \tan(\phi) f_c + \frac{2}{\pi\beta D} (T_1^2 + T_2^2) \quad 2\tilde{\sigma}_{tt} \right] \quad (5.52)$$

$$\mathbf{m} = \frac{\partial Q}{\partial \boldsymbol{\sigma}} \quad (5.53)$$

$$\mathbf{m} = \left[2T_3 \tan(\phi) f_c + \frac{2}{\pi\beta D} (T_3^2 - T_4^2) \quad 2\tilde{\sigma}_{tt} \right] \quad (5.54)$$

$$\dot{q}_u = \boldsymbol{\omega}_u \dot{\lambda} \quad (5.55)$$

$$\boldsymbol{\omega}_u := (\partial \mathbf{q}_u / \partial \mathbf{W}^p) (\partial \mathbf{W}^p / \partial \boldsymbol{\epsilon}^p) (\partial \boldsymbol{\epsilon}^p / \partial \lambda) = (\partial \mathbf{q}_u / \partial \mathbf{W}^p)_{(6,4)} \mathbf{H}_{(4,2)} \mathbf{m}_{(2,1)} \quad (5.56)$$

$$H = \partial \mathbf{W}^p / \partial \boldsymbol{\epsilon}^p \quad (5.57)$$

$$\mathbf{H} = \begin{bmatrix} \langle \tilde{\sigma}_{nn} \rangle & O \\ 0 & \tilde{\sigma}_{tt} - \sigma_{\mathbf{ttr1}} \text{sign}(\sigma_{tt}) \\ 0 & \sigma_{\mathbf{ttr1}} - \sigma_{\mathbf{ttr2}} \text{sign}(\sigma_{tt}) \\ \langle \langle \tilde{\sigma}_{nn} \rangle \rangle & 0 \end{bmatrix} \quad (5.58)$$

$$\varpi = \left[\begin{array}{l} (-m_1 \mathbf{H}(1, 1) \frac{\beta_C}{G_f^I} - m_2 \mathbf{H}(2, 2) \frac{\beta_C}{G_f^{II}})(C_0 - C_r) \exp^{-\beta_C \left(\frac{w_1^p}{G_f^I} + \frac{w_2^p}{G_f^{II}} \right)} \\ (-m_1 \mathbf{H}(1, 1) \frac{\beta_C}{G_f^I} - m_2 \mathbf{H}(2, 2) \frac{\beta_C}{G_f^{II}})(C_{Q_0} - C_{Q_r}) \exp^{-\beta_{C_Q} \left(\frac{w_1^p}{G_f^I} + \frac{w_2^p}{G_f^{II}} \right)} \\ -m_2 \mathbf{H}(3, 2) \beta_\phi (\phi_0 - \phi_r) \exp^{-\beta_\phi w_3^p} \\ -m_2 \mathbf{H}(3, 2) \beta_\psi (\psi_0 - \psi_r) \exp^{-\beta_\psi w_3^p} \\ (-m_1 \mathbf{H}(1, 1) \frac{\beta_\zeta}{G_f^I} - m_2 \mathbf{H}(2, 2) \frac{\beta_\zeta}{G_f^{II}}) \xi_0 \exp^{-\beta_\xi \left(\frac{w_1^p}{G_f^I} + \frac{w_2^p}{G_f^{II}} \right)} \\ m_1 \mathbf{H}(4, 1) \frac{\partial \zeta}{\partial w_4} \end{array} \right] \quad (5.59)$$

$$\zeta = \begin{cases} \zeta_0 + (\zeta_p - \zeta_0) \sqrt{\left(\frac{2w_4^p}{w_p} \right) - \left(\frac{w_4^p}{w_p} \right)^2} & \text{if } w_4^p \leq w_p \\ \zeta_0 + (\zeta_p - \zeta_r) \left(\frac{w_4^p - w_p}{w_m - w_p} \right)^2 & \text{if } w_p \leq w_4^p \leq w_m \\ \zeta_r + (\zeta_m - \zeta_r) \exp^{\beta_\zeta \left(\frac{w_4^p - w_p}{\zeta_m - \zeta_r} \right)} & \text{if } w_4^p > w_m \end{cases} \quad (5.60)$$

$$\frac{\partial \zeta}{\partial w_4} = \quad (5.61)$$

5.2.4 Jacobian Terms

$$\frac{\partial \mathbf{r}_1}{\partial \boldsymbol{\sigma}} = I + \lambda K \frac{\partial \mathbf{m}}{\partial \boldsymbol{\sigma}} \quad (5.62)$$

$$\frac{\partial \mathbf{r}_1}{\partial q_{ui}} = \lambda K \frac{\partial \mathbf{m}}{\partial q_{ui}} \quad (5.63)$$

$$\frac{\partial \mathbf{r}_1}{\partial a_i} = 0 \quad (5.64)$$

$$\frac{\partial \mathbf{r}_1}{\partial \kappa_u} = 0 \quad (5.65)$$

$$\frac{\partial \mathbf{r}_1}{\partial \lambda} = Km \quad (5.66)$$

$$\frac{\partial \mathbf{m}}{\partial \boldsymbol{\sigma}} = \begin{bmatrix} -2f_c \tan^2 \psi + \frac{8}{\pi^* \beta D} \tan \psi T_3 + \frac{4(\sigma_{nn} - \zeta)}{\pi \beta^3 D^2} (T_3^2 - T_4^2) & 0 \\ 0 & 2 \end{bmatrix} \quad (5.67)$$

$$\frac{\partial \mathbf{m}}{\partial C_Q} = \begin{bmatrix} 2f_c \tan \psi + \frac{4}{\pi^* \beta D} (T_4 - T_3) \\ 0 \end{bmatrix} \quad (5.68)$$

$$\frac{\partial \mathbf{m}}{\partial \xi} = \begin{bmatrix} \frac{4}{\pi^* \beta D} \tan \psi T_4 \\ 0 \end{bmatrix} \quad (5.69)$$

$$\frac{\partial \mathbf{m}}{\partial \zeta} = \begin{bmatrix} 2f_c \sec^2 \psi (T_3 - \sigma_{nn} \tan \psi) + \frac{4}{\pi^* \beta D} \sec^2 \psi + (\sigma_{nn} T_3 - 4) \\ 0 \end{bmatrix} \quad (5.70)$$

$$\frac{\partial \mathbf{m}}{\partial C} = \frac{\partial \mathbf{m}}{\partial \phi} = 0 \quad (5.71)$$

$$\frac{\partial \mathbf{r}_3}{\partial \sigma} = -\lambda \frac{\partial \mathbf{1}}{\partial \sigma} \quad (5.72)$$

$$\frac{\partial \mathbf{1}}{\partial \sigma} = \begin{bmatrix} \frac{\beta_C}{G_f^I} (C_0 - C_r) \exp \left(-\beta_C \left(\frac{w_1^p}{G_f^I} + \frac{w_2^p}{G_f^{II}} \right) \right) \left(\frac{\partial m_1}{\partial \sigma_{nn}} < \sigma_{nn} > + \frac{m_1}{2} (1 + \text{sign}(\tilde{\sigma}_{nn})) \right) \\ \frac{\beta_C}{G_f^{II}} (C_0 - C_r) \exp \left(-\beta_C \left(\frac{w_1^p}{G_f^I} + \frac{w_2^p}{G_f^{II}} \right) \right) \left(\frac{\partial m_2}{\partial \sigma_{tt}} (\tilde{\sigma}_{tt} - \sigma_{ttr1} \text{sign}(\tilde{\sigma}_{tt})) + m_2 \right) \end{bmatrix} \quad (5.73)$$

$$\frac{\partial \mathbf{r}_3}{\partial q_{ui}} = \delta \frac{\beta_C}{G_f^I} (C_0 - C_r) \exp \left(-\beta_C \left(\frac{w_1^p}{G_f^I} + \frac{w_2^p}{G_f^{II}} \right) \right) \left(\frac{\partial m_1}{\partial q_{ui}} < \sigma_{nn} > q_{ui} = C_Q, \xi, \zeta, \psi \right) \quad (5.74)$$

$$\frac{\partial r_3}{\partial C} = 1, \frac{\partial r_3}{\partial \phi} = 0, \frac{\partial r_3}{\partial \Delta \lambda} = \varpi_1, \quad (5.75)$$

$$\frac{\partial \mathbf{r}_3}{\partial a_i} = 0 \quad (5.76)$$

$$\frac{\partial \mathbf{r}_3}{\partial \kappa_u} = 0 \quad (5.77)$$

$$\frac{\partial \mathbf{r}_3}{\partial \lambda} = -\varpi \quad (5.78)$$

$$\frac{\partial \mathbf{r}_4}{\partial \sigma} = -\Delta \frac{\partial \varpi_2}{\partial \sigma} \quad (5.79)$$

$$\frac{\partial \varpi_2}{\partial \sigma} = \begin{bmatrix} \frac{\beta_{CQ}}{G_f^I} (C_{Q0} - C_{Qr}) \exp \left(-\beta_{CQ} \left(\frac{w_1^p}{G_f^I} + \frac{w_2^p}{G_f^{II}} \right) \right) \left(\frac{\partial m_1}{\partial \sigma_{nn}} < \sigma_{nn} > + \frac{m_1}{2} (1 + \text{sign}(\tilde{\sigma}_{nn})) \right) \\ \frac{\beta_{CQ}}{G_f^{II}} (C_{Q0} - C_{Qr}) \exp \left(-\beta_{CQ} \left(\frac{w_1^p}{G_f^I} + \frac{w_2^p}{G_f^{II}} \right) \right) \left(\frac{\partial m_2}{\partial \sigma_{tt}} (\tilde{\sigma}_{tt} - \sigma_{ttr1} \text{sign}(\tilde{\sigma}_{tt})) + m_2 \right) \end{bmatrix} \quad (5.80)$$

$$\frac{\partial \mathbf{r}_4}{\partial C_Q} = 1 + \Delta \lambda \frac{\beta_{CQ}}{G_f^I} (C_{Q0} - C_{Qr}) \exp \left(-\beta_{CQ} \left(\frac{w_1^p}{G_f^I} + \frac{w_2^p}{G_f^{II}} \right) \right) \left(\frac{\partial m_1}{\partial C_Q} < \sigma_{nn} > \right) \quad (5.81)$$

$$\frac{\partial \mathbf{r}_4}{\partial q_{ui}} = \Delta \lambda \frac{\beta_{CQ_0}}{G_f^I} (C_Q - C_{Qr}) \exp \left(-\beta_{CQ} \left(\frac{w_1^p}{G_f^I} + \frac{w_2^p}{G_f^{II}} \right) \right) \left(\frac{\partial m_1}{\partial C_Q} < \sigma_{nn} > \right) \quad (5.82)$$

$$\frac{\partial r_4}{\partial C} = 0, \frac{\partial r_4}{\partial \phi} = 0, \frac{\partial r_4}{\partial \Delta \lambda} = \varpi_2, \quad (5.83)$$

$$\frac{\partial \mathbf{r}_4}{\partial a_i} = 0 \quad (5.84)$$

$$\frac{\partial \mathbf{r}_4}{\partial \kappa_u} = 0 \quad (5.85)$$

$$\frac{\partial \mathbf{r}_4}{\partial \lambda} = \varpi_2 \quad (5.86)$$

$$\frac{\partial \mathbf{r}_5}{\partial \sigma} = \Delta \frac{\partial \varpi_3}{\partial \sigma} \quad (5.87)$$

$$\frac{\partial \varpi_3}{\partial \sigma} = \left[\begin{array}{l} \frac{\beta_\xi}{G_f^I} \xi_0 \exp \left(-\beta_\xi \left(\frac{w_1^p}{G_f^I} + \frac{w_2^p}{G_f^{II}} \right) \right) \left(\frac{\partial m_1}{\partial \sigma_{nn}} \langle \sigma_{nn} \rangle + \frac{m_1}{2} (1 + \text{sign}(\tilde{\sigma}_{nn})) \right) \\ \frac{\beta_\xi}{G_f^{II}} \xi_0 \exp \left(-\beta_\xi \left(\frac{w_1^p}{G_f^I} + \frac{w_2^p}{G_f^{II}} \right) \right) \left(\frac{\partial m_2}{\partial \sigma_{tt}} (\tilde{\sigma}_{tt} - \sigma_{ttr1} \text{sign}(\tilde{\sigma}_{tt})) + m_2 \right) \end{array} \right] \quad (5.88)$$

$$\frac{\partial \mathbf{r}_5}{\partial q_{ui}} = \Delta \lambda \frac{\beta_\xi}{G_f^I} \beta_\xi \exp \left(-\beta_\xi \left(\frac{w_1^p}{G_f^I} + \frac{w_2^p}{G_f^{II}} \right) \right) \left(\frac{\partial m_1}{\partial q_{ui}} \langle \sigma_{nn} \rangle, q_{ui} = C_Q, \zeta, \psi \right) \quad (5.89)$$

$$\frac{\partial \mathbf{r}_5}{\partial \xi} = 1 + \Delta \lambda \frac{\beta_\xi}{G_f^I} \beta_\xi \exp \left(-\beta_\xi \left(\frac{w_1^p}{G_f^I} + \frac{w_2^p}{G_f^{II}} \right) \right) \left(\frac{\partial m_1}{\partial \xi} \langle \sigma_{nn} \rangle \right) \quad (5.90)$$

$$\frac{\partial \mathbf{r}_5}{\partial C} = 0, \frac{\partial \mathbf{r}_5}{\partial \phi} = 0, \frac{\partial \mathbf{r}_5}{\partial \Delta \lambda} = \varpi_3, \quad (5.91)$$

$$\frac{\partial \mathbf{r}_5}{\partial a_i} = 0 \quad (5.92)$$

$$\frac{\partial \mathbf{r}_5}{\partial \kappa_u} = 0 \quad (5.93)$$

$$\frac{\partial \mathbf{r}_5}{\partial \lambda} = \varpi_3 \quad (5.94)$$

$$\frac{\partial \mathbf{r}_6}{\partial \sigma} = -\Delta \frac{\partial \varpi_4}{\partial \sigma} \quad (5.95)$$

$$\frac{\partial \varpi_4}{\partial \sigma} = \left[\begin{array}{l} \frac{\partial \zeta}{\partial w_4} \left(\frac{\partial m_1}{\partial \sigma_{nn}} \langle \langle \tilde{\sigma}_{nn} - \zeta_{nn} \rangle \rangle + \frac{m_1}{2} (1 + \text{sign}(\tilde{\sigma}_{nn} - \zeta_{nn})) \right) \\ 0 \end{array} \right] \quad (5.96)$$

$$\frac{\partial \mathbf{r}_6}{\partial q_{ui}} = \Delta \lambda \frac{\partial m_1}{\partial q_{ui}} \langle \langle \tilde{\sigma}_{nn} \rangle \rangle, q_{ui} = C_Q, \xi, \psi \quad (5.97)$$

$$\frac{\partial \mathbf{r}_6}{\partial \zeta} = 1 + \Delta \lambda \frac{\partial \zeta}{\partial w_4} \frac{\partial m_1}{\partial q_{ui}} \langle \langle \tilde{\sigma}_{nn} - \zeta_m \rangle \rangle \quad (5.98)$$

$$\frac{\partial \mathbf{r}_6}{\partial C} = 0, \frac{\partial \mathbf{r}_6}{\partial \phi} = 0, \frac{\partial \mathbf{r}_6}{\partial \Delta \lambda} = \varpi_4, \quad (5.99)$$

$$\frac{\partial \mathbf{r}_6}{\partial a_i} = 0 \quad (5.100)$$

$$\frac{\partial \mathbf{r}_6}{\partial \kappa_u} = 0 \quad (5.101)$$

$$\frac{\partial \mathbf{r}_6}{\partial \lambda} = \varpi_4 \quad (5.102)$$

$$\frac{\partial \mathbf{r}_7}{\partial \sigma} = \Delta \lambda \frac{\partial \varpi_5}{\partial \sigma} \quad (5.103)$$

$$\frac{\partial \varpi_5}{\partial \sigma} = \begin{bmatrix} 0 \\ -\beta_\phi(\sigma_{\tilde{t}r1} - \sigma_{\tilde{t}r2})\text{sign}(\tilde{\sigma}_{\tilde{t}t})(\phi_0 - \phi_r)e^{-\beta_\phi} \frac{\partial m_2}{\partial \sigma_{\tilde{t}t}} \end{bmatrix} \quad (5.104)$$

$$\frac{\partial \mathbf{r}_7}{\partial q_{ui}} = 0 \quad (5.105)$$

$$\frac{\partial r_7}{\partial \phi} = 0, \frac{\partial r_7}{\partial \Delta \lambda} = -\varpi_5, q_{ui} = C, C_Q, \xi, \psi, \zeta \quad (5.106)$$

$$\frac{\partial \mathbf{r}_7}{\partial a_i} = 0 \quad (5.107)$$

$$\frac{\partial \mathbf{r}_7}{\partial \kappa_u} = 0 \quad (5.108)$$

$$\frac{\partial \mathbf{r}_7}{\partial \lambda} = \varpi_5 \quad (5.109)$$

$$\frac{\partial \mathbf{r}_8}{\partial \sigma} = \Delta \frac{\partial \varpi_6}{\partial \sigma} \quad (5.110)$$

$$\frac{\partial \varpi_6}{\partial \sigma} = \begin{bmatrix} 0 \\ -\beta_\psi(\sigma_{\tilde{t}r1} - \sigma_{\tilde{t}r2})\text{sign}(\tilde{\sigma}_{\tilde{t}t})(\psi_0 - \psi_r)e^{-\beta_\psi} \frac{\partial m_2}{\partial \sigma_{\tilde{t}t}} \end{bmatrix} \quad (5.111)$$

$$\frac{\partial \mathbf{r}_8}{\partial q_{ui}} = 0 \quad (5.112)$$

$$\frac{\partial r_7}{\partial \psi} = 0, \frac{\partial r_7}{\partial \Delta \lambda} = -\varpi_6, q_{ui} = C, C_Q, \xi, \phi, \zeta \quad (5.113)$$

$$\frac{\partial \mathbf{r}_8}{\partial a_i} = 0 \quad (5.114)$$

$$\frac{\partial \mathbf{r}_8}{\partial \kappa_u} = 0 \quad (5.115)$$

$$\frac{\partial \mathbf{r}_8}{\partial \lambda} = \varpi_6 \quad (5.116)$$

$$\frac{\partial \mathbf{r}_9}{\partial \sigma} = 0 \quad (5.117)$$

$$\frac{\partial \mathbf{r}_9}{\partial q_{ui}} = 0 \quad (5.118)$$

$$\frac{\partial \mathbf{r}_9}{\partial a_1} = I(\text{first component of backstress}) \quad (5.119)$$

$$\frac{\partial \mathbf{r}_9}{\partial \lambda} = -(1 - M)(K_{ks} \mathbf{u}_\alpha) \quad (5.120)$$

$$\frac{\partial \mathbf{r}_{10}}{\partial \sigma} = 0 \quad (5.121)$$

$$\frac{\partial \mathbf{r}_{10}}{\partial q_{ui}} = 0 \quad (5.122)$$

$$\frac{\partial \mathbf{r}_{10}}{\partial a_1} = 0 \quad (5.123)$$

$$\frac{\partial \mathbf{r}_{10}}{\partial \lambda} = -(1 - M)(K_{ks} \mathbf{u}_\alpha) \quad (5.124)$$

$$\frac{\partial \mathbf{r}_{11}}{\partial \boldsymbol{\sigma}} = \frac{\partial \boldsymbol{\kappa}_u}{\partial \boldsymbol{\sigma}} \quad (5.125)$$

$$\frac{\partial \mathbf{r}_{11}}{\partial q_{ui}} = 0 \quad (5.126)$$

$$\frac{\partial \mathbf{r}_{11}}{\partial a_i} = 0 \quad (5.127)$$

$$\frac{\partial \mathbf{r}_{11}}{\partial \kappa_u} = 1 \quad (5.128)$$

$$\frac{\partial \mathbf{r}_{11}}{\partial \lambda} = -1 \quad (5.129)$$

$$\frac{\partial \mathbf{r}_{12}}{\partial \boldsymbol{\sigma}} = -\frac{\partial \mathbf{F}}{\partial \boldsymbol{\sigma}} = n \quad (5.130)$$

$$(5.131) \quad \frac{\partial r_{12}}{\partial C} = 2f_c(T_2 - T_1), \quad \frac{\partial r_{12}}{\partial \xi} = 2f_c(T_2 \tan \phi) \frac{\partial r_{12}}{\partial \phi} = 2f_c \sec^2 \phi (T_1 \bar{\sigma} - T_2 \xi)$$

$$\frac{\partial \mathbf{r}_{12}}{\partial a_i} = 0 \quad (5.132)$$

$$\frac{\partial \mathbf{r}_{12}}{\partial \kappa_u} = 0 \quad (5.133)$$

$$\frac{\partial \mathbf{r}_{12}}{\partial \lambda} = 0 \quad (5.134)$$

5.2.5 Algorithmic Implementation

Steps

1. At current increment variables known are

$$\boldsymbol{\sigma}_n, \mathbf{a}_n \mathbf{q}_{u,n}, \mathbf{W}_n^p, \boldsymbol{\epsilon}_n^p$$

2. Strain driven process results in an elastic predictor and plastic corrector step. The elastic Predictor step where plastic flow is frozen during the finite step is

$$\boldsymbol{\sigma}_{n+1}^{trial} = \boldsymbol{\sigma}_n + \mathbf{K} \Delta \boldsymbol{\epsilon}$$

$$\boldsymbol{\epsilon}_{n+1}^{trial} = \boldsymbol{\epsilon}_n$$

$$\mathbf{a}_{n+1}^{trial} = \mathbf{a}_n$$

$$\mathbf{q}_{n+1}^{trial} = \mathbf{q}_n$$

$$\kappa_{u,n+1}^{trial} = \kappa_{un}$$

$$(5.135) \quad F_{u,n+1}^{trial} = F_{u,n+1}(\boldsymbol{\sigma}_{n+1}^{trial}, \mathbf{q}_{n+1}^{trial} \mathbf{a}_{n+1}^{trial}, \kappa_{u,n+1}^{trial})$$

3. Compute the yield function $F^{trial}(\boldsymbol{\sigma}_{n+1}^{trial}, \mathbf{q}_n, \mathbf{a}_{n+1}^{trial}, \kappa_{u,n+1}^{trial})$

4. Check for the yield condition

$$F^{trial}(\boldsymbol{\sigma}_{n+1}^{trial}, \mathbf{q}_n, \mathbf{a}_{n+1}^{trial}) < 0 \quad \text{Elastic State}$$

$$\text{update } \boldsymbol{\sigma}_{n+1} = \boldsymbol{\sigma}_{n+1}^{trial};$$

$$\text{update } \tilde{\boldsymbol{\sigma}}_{n+1} = \tilde{\boldsymbol{\sigma}}_{n+1}^{trial};$$

$$\text{update } \mathbf{q}_{n+1} = \mathbf{q}_n;$$

$$\text{update } \mathbf{W}_{n+1}^p = \mathbf{W}_n^p;$$

$$\text{update } \mathbf{a}_{n+1}^{trial} = \mathbf{a}_n;$$

$$\text{update } \boldsymbol{\epsilon}_{n+1}^p = \boldsymbol{\epsilon}_n^p;$$

$$\text{update } \kappa_{u,n+1}^{trial} = \kappa_{un}$$

5. For a Stress reversal cases CT or TC

After a plastic process (monotonic or cyclic), A stress reversal case is established under the condition of a negative unloading yield function value unloading movements CT or TC must be started from the respective monotonic envelope whenever, after a converged load step where

$$F_n(\boldsymbol{\sigma}_n, \mathbf{q}_n) = 0$$

The following condition occurs

$$F_{n+1}^{trial} = F_{n+1}(\boldsymbol{\sigma}_{n+1}^{trial}, \mathbf{q}_{n+1}^{trial}) < 0$$

6. For Remaining cases CTC or TCT.

After a converged load step where

$$F_{u,n}(\boldsymbol{\sigma}_n, \mathbf{a}_n, q_{u,n}) < 0$$

The following condition occurs

$$F_{u,n+1}^{trial} = F_{u,n+1}(\boldsymbol{\sigma}_{n+1}^{trial}, \mathbf{a}_{n+1}^{trial}, q_{u,n+1}^{trial}) < 0$$

$$r(\boldsymbol{\sigma}_{n+1}, \mathbf{q}_{n+1}, \mathbf{a}_{n+1}, \Delta\lambda_{u,n+1}) = \begin{cases} \boldsymbol{\sigma}_{n+1} - \boldsymbol{\sigma}_{n+1}^{trial} + \Delta\lambda_{u,n+1} \mathbf{K} \mathbf{m}_{n+1} = 0 \\ \mathbf{q}_{u,n+1} - \mathbf{q}_{u,n} + \Delta\lambda_{u,n+1} \boldsymbol{\varpi}_{u,n+1} = 0 \\ \mathbf{a}_{n+1} - \mathbf{a}_n - (1 - M) \Delta\lambda_{u,n+1} \mathbf{K}_{secant} \mathbf{u}_{a,n+1} = 0 \\ F(\boldsymbol{\sigma}_{n+1}, \mathbf{q}_{u,n+1}, \mathbf{a}_{n+1}) = 0 \\ \kappa_{u,n+1} - \kappa_{u,n} - \Delta\lambda_{u,n+1} = 0 \end{cases} \quad (5.136)$$

7. Plastic Corrector step

The system of non-linear equations expressed by above equations .It can be significantly simplified because the variables $\boldsymbol{\sigma}_{n+1}$, \mathbf{q}_{n+1} and \mathbf{W}_{n+1}^p ; \mathbf{a}_{n+1} , $\boldsymbol{\epsilon}_{n+1}^p$ can be expressed as functions of $\Delta\lambda_{u,n+1}$ and, therefore, above is transformed into a non-linear equation of one single variable

Discrete Kuhn Tucker Conditions to be applied

$$\Delta\lambda_{u,n+1} \geq 0, F_{u,n+1}(\boldsymbol{\sigma}_{n+1}, \mathbf{a}_{n+1}, q_{u,n+1}, \kappa_{u,n+1}) \leq 0$$

$$\Delta\lambda_{u,n+1} F_{u,n+1}(\boldsymbol{\sigma}_{n+1}, \mathbf{a}_{n+1}, q_{u,n+1}, \kappa_{u,n+1}) = 0$$

Each time a stress reversal takes place, a new unloading surface is activated, being deactivated when it reaches the monotonic envelope towards which it moves, thus, for the same load step, yielding may occur both on the unloading surface and on the monotonic surface.

8. Sub-incremental procedure

Therefore, a sub-incremental procedure must be used in order to split such load increment into two sub-increments, each one corresponding to a different yield surface. In a strain driven process, in

which the total strain vector is the only independent variable

Scalar $0 < y < 1$ should be computed such that the following condition satisfies $\epsilon_{n+1} = \epsilon_n + y\epsilon_{n+1} + (1 - y)\epsilon_{n+1}$

$y\epsilon_{n+1}$ = leads the unloading surface to touch the monotonic one.

$(1 - y)\epsilon_{n+1}$ = After deactivation of unloading surface strain increment , this increment is used for the monotonic surface

y is computed through the bisection method, where the monotonic yield function is evaluated at each iteration.

Chapter 6

Verification Examples

6.1 Verification Examples for Monotonic Loading

In order to verify the proposed composite interface model various verification examples have been considered in this section. The formulated constitutive model is verified by implementing a single zero-thickness interface, which is a 4-node two dimensional cohesive element with two integration point. The material parameter used for verification are tabulated in Table obtained from the calibration process. Specifically, to find the values of mode I and mode II fracture energy, it is assumed that $G_f^I = 5G_{f,min}^I$ and $G_f^{II} = 10G_f^I$, where $G_{f,min}^I = \xi_0^2/2k_{nn}$ corresponding to the perfectly brittle tensile fracture. The verification examples include interface in tension, compression and shear mode condition. The implementation is done in ABAQUS, by using the user defined subroutine (UMAT).[35]

Direct tension test

In this test the interface is subjected to direct tension. A normal relative displacement is applied to the nodes on the top face of the interface element while all the degrees of freedom on the bottom face are fixed. shows the variation of tensile strength ξ with mix mode fracture energy $\frac{w_1^p}{G_f^I} + \frac{w_2^p}{G_f^{II}}$. The response exhibits a exponential degradation of the tensile strength and matches well with the analytical values.

Direct compression test

In this test the interface is subjected to direct compression. The test is performed to check the functionality of the compression cap. A normal relative displacement is applied to produce the pure compression state in the interface and variation of compression strength (ζ) with work hardening

Table 6.1: Elastic material property for the Brick and joints

Brick		Joint	
E	ν	k_{nn}	k_{tt}
N/mm^2		N/mm^3	N/mm^3
2000	0.15	1000	1000

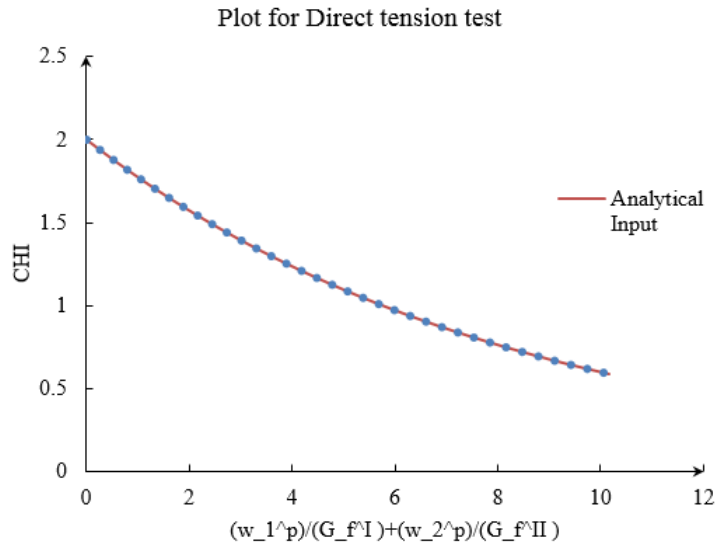


Figure 6.1: Plot of distribution of tensile strength ξ with $\left(\frac{w_1^p}{G_f^I} + \frac{w_2^p}{G_f^II}\right)$.

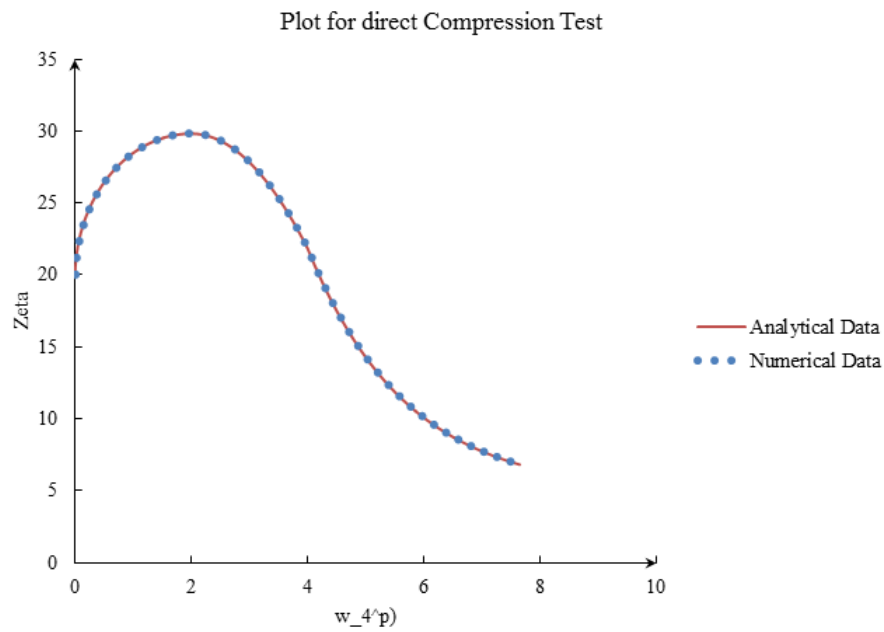


Figure 6.2: Plot of distribution of compression strength ζ with w_4^p .

Table 6.2: Inelastic material property for the joints

Tension	$\xi_0 [N/mm^2]$ $G_f^I [Nmm/mm^2]$	2 $5\xi_0^2/2K_{nn}$
Shear	$C_0 \setminus C_r [N/mm^2]$	$1.4\xi_0 \setminus 0.1C_Q$
	$C_{Q0} \setminus C_{Qr} [N/mm^2]$	$1.1\xi_0 \setminus 0.1C_Q$
	$\phi_0 \setminus \phi_r [radian]$	$0.65 \setminus 0.50$
	$\psi_0 \setminus \psi_r [radian]$	$0.30 \setminus 0.20$
	$G_f^{II} [Nmm/mm^2]$	$10G_f^I$
Cap	$\zeta_p [N/mm^2]$	30

parameter w_4^p is traced and compared with the analytical values by solving Equation [22](zeta). It can be observed from Figure , that the internal hardening variable (ζ) coincides well with the analytical values.

Chapter 7

Applications of proposed Model

The numerical model has to be validated by comparisons with experimental results. However, available experimental results performed under cyclic loading in cementitious interfaces are scarce, especially experiments performed under tensile loading. Therefore, comparison will be done using masonry and concrete test results. It is important to note that the failure of the interface element under tensile loading is directly related with the failure of the mortar joint, but its failure under compressive loading is associated with the failure of the unit and mortar joint. The ability of the proposed constitutive model to simulate experimental results is next assessed by a comparison with reputed available experimental data obtained under several loading conditions

7.1 Behavior of Interface during cyclic loading

The Behavior of Interface under cyclic loading is shown where elastic unloading and non linear unloading or reloading is observed based on the cyclic strains .Numerical tests were conducted on a Zero thickness Cohesive element (COH2D) to which has 2 integration points. using Abaqus 6.10 Version

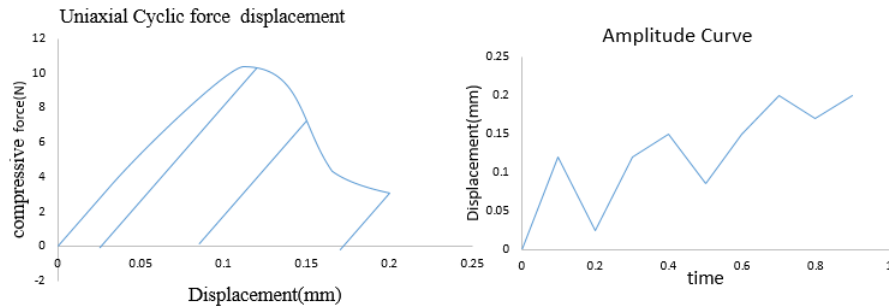
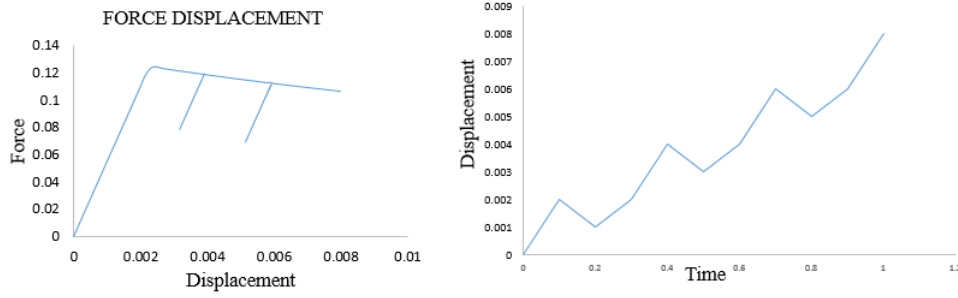


Figure 7.1: Uniaxial Cyclic Compression force displacement curve for the Mortar Interface



Uniaxial

Cyclic Interface Displacement controlled test in tension

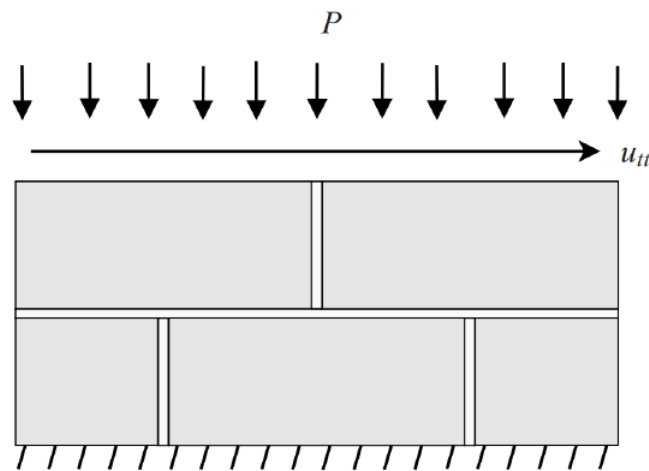


Figure 7.2: Direct Shear test set up Atkinson et al

7.1.1 Behavior Of Interface in uniaxial Tension and Compression

Cyclic displacements were imposed uniaxially as shown in Amplitude curves and the Proposed model here is capable of producing the elastic unloading for the given strains ,Similarly Uniaxial cyclic tensile displacement controlled test is performed numerically

7.2 Direct shear test

A direct shear test on mortar joints carried out by Atkinson et al. (1989) is used here to evaluate the ability of the model to predict cyclic shear loading assuming elastic unloading/reloading behaviour. The comparison between experimental data and numerical response is shown in Figure. The results were scaled by the experimental values at peak. A good agreement can be found between the experimental and the numerical results. As assumed at the formulation of the constitutive model, elastic behaviour for shear unloading/reloading showed to be a good approximation to experiments.

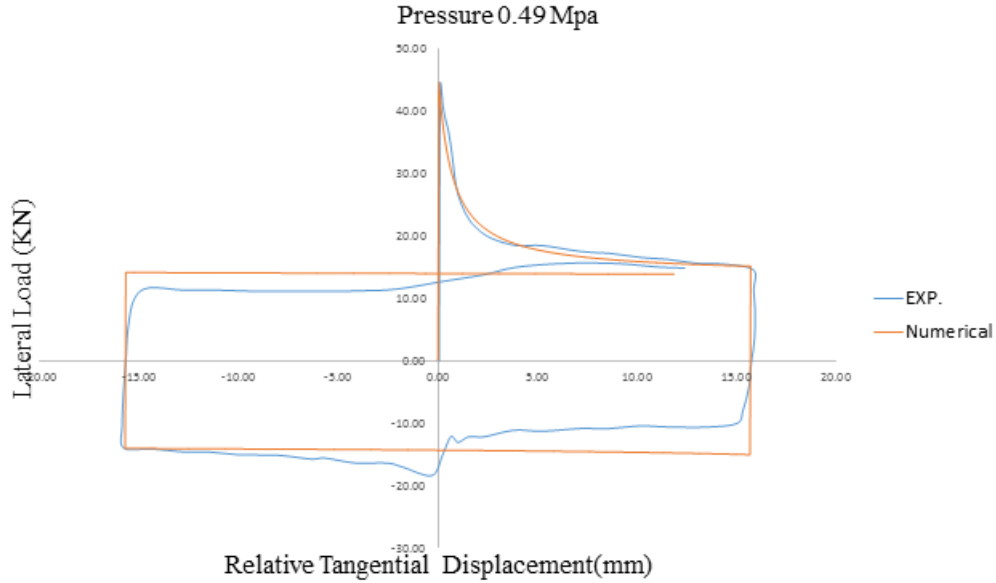


Figure 7.3: Comparison between experimental results from direct shear test atkinson1989 and Numerical results obtained from the present model (a) $P = 0.49$ MPa; (b) distribution of normal displacements with relative tangential displacements for different pressure.

Masonry bed joints in direct cyclic shear loading

Atkinson conducted direct shear tests using a servo-controlled loading apparatus to examine the response of brick masonry bed joints under monotonic and cyclic shear loadings. In each of these tests, first a uniformly distributed normal stress and then four cycles of shear reversals were imposed under displacement control. The specimens consist of modern clay bricks [$193 \times 55 \times 92 \text{ mm}^3$] and mortar joints [7 mm], prepared with a volumetric cement : lime : sand ratio (1 : 1.5 : 4.5). The bed joint area is equal to $92 \times 398 \text{ mm}^2 (0.037 \text{ m}^2)$.

The comparison between numerical and experimental load-displacement curves is shown in Figure 7.3, which shows that the proposed model is able to reproduce the shear behaviour of brick masonry bed joints not only in monotonic but also in cyclic loading. The experimental and numerical dilatancy curves show that, higher the compressive stress, smaller is the dilatancy and it is observed that the correlation of numerical and experimental results is good. When the interface between the elastic region (elastic brick) is subjected to shear deformations under a normal confinement, Initially the normal stress on the interface is zero. However, since the elastic boundary prevents the interface from dilating freely, a significant compressive stress develops on the interface during the application of relative tangential displacement.

7.3 Behavior of a two Brick model in Monotonic and Cyclic loading

The proposed Zero interface is used in the Simplified Modelling where the the brick units are expanded into the mortar thickness and the cyclic displacement tests are conducted numerically in

both tension and compression CPS4R elements with Gauss integration scheme is used for modelling the Brick units with the below mentioned elastic units and for Mortar is modeled using a Cohesive 2D element in Abaqus

7.3.1 Monotonic Behavior

The Monotonic Force displacement behavior is also produced to show the capability of the model in producing the cyclic behavior uniaxially in both tension and compression cases all force units are in N and Displacements are in mm unless specified

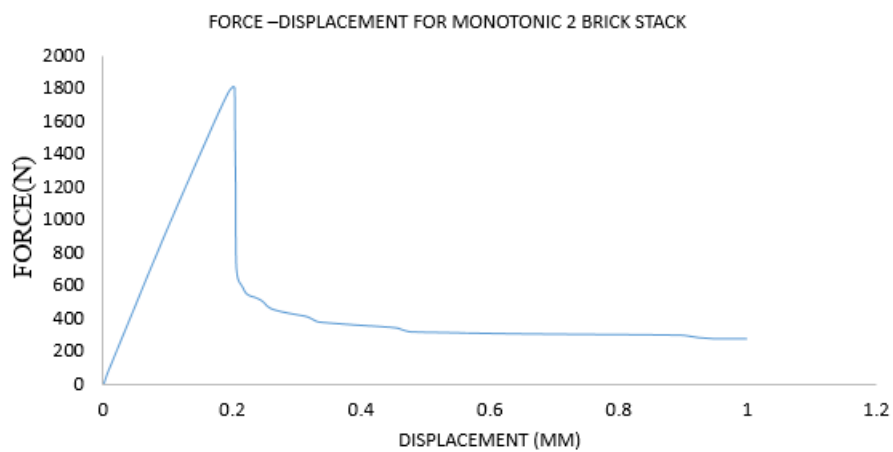


Figure 7.4: Monotonic force displacement curve for the Model in Compression (Displacement controlled)

7.3.2 Cyclic behavior of a two brick model

Cyclic displacements are imposed for the model at the top of the brick and the force displacement plots are produced to show the capability of the model in producing nonlinearity during unloading and reloading. The Properties udes are as below in table

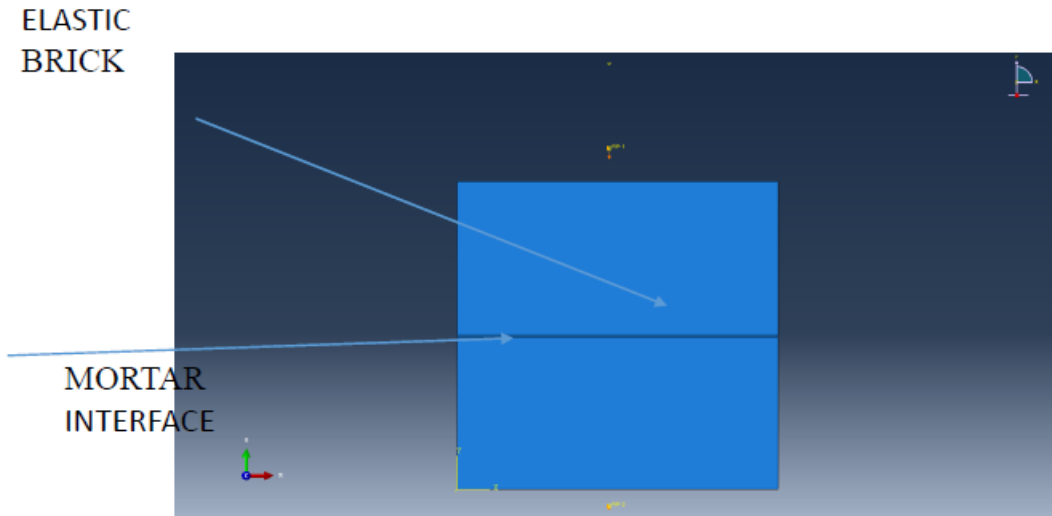


Figure 7.5: Two brick Model with the the proposed zero thickness interface Model

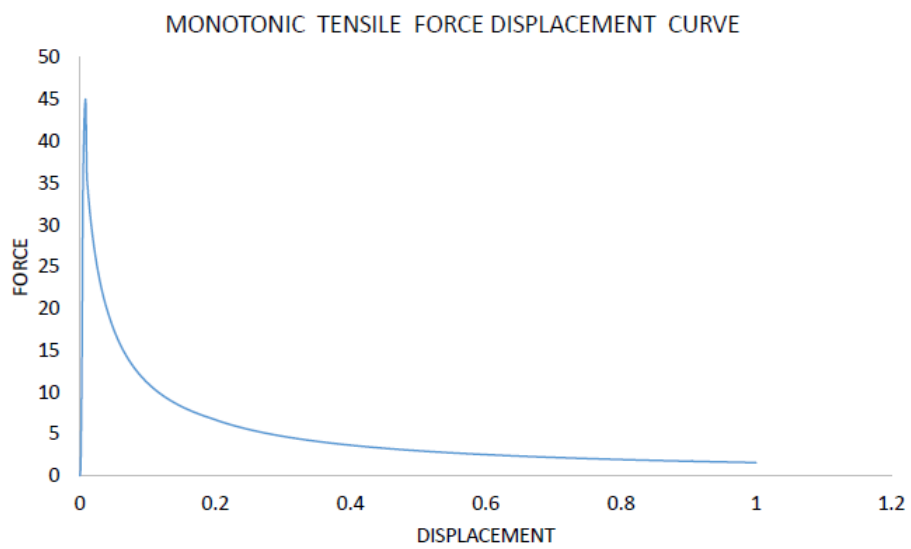


Figure 7.6: Monotonic behavior of the Two brick Model in Tension

	Unit	Interface	
E [N/mm ²]	Poissons ratio	k _n [N/mm ³]	[N/mm ³]
16700	0.20	110	50

Figure 7.7: Material Parameters adopted

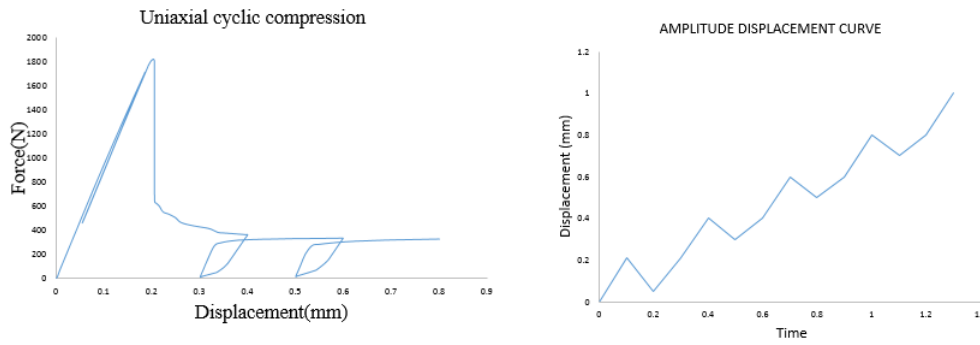


Figure 7.8: Cyclic force displacement curve for two brick stack under Compression

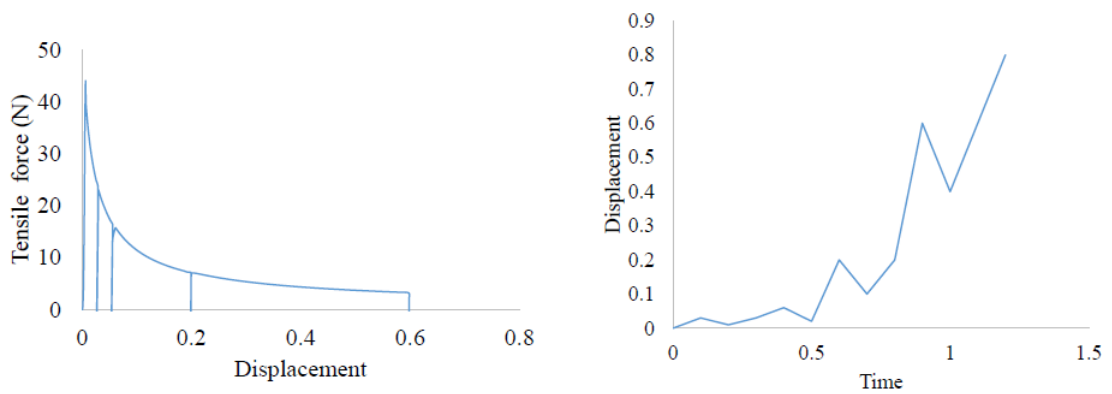


Figure 7.9: Cyclic force displacement curve for two brick stack under Tension

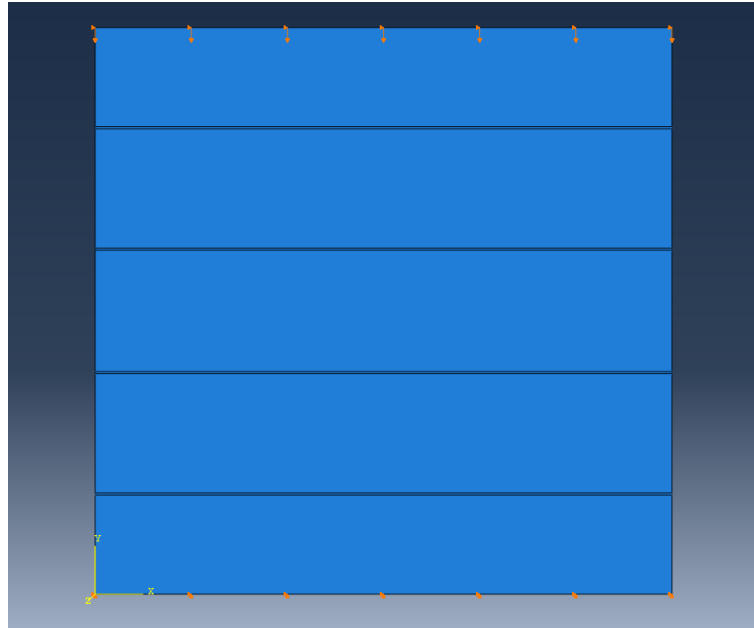


Figure 7.10: Brick prism model(UPC BP1) subjected to displacement controlled cyclic test

7.4 UPC stacked bond prisms

The first group concerns the analysis of two stacked bond prisms, tested under cyclic loading at Universitat Politècnica de Catalunya. stacked bond prisms of five bricks each, named BP1, were constructed and tested under cyclic loading until failure was reached. Modelling resorts to four node zero-thickness line interface elements for the mortar joints and eight-node continuum plane stress elements for the brick units, as illustrated in Figure Numerical tests are performed under displacement controlled tests by imposing the vertical displacements over the top edge and the horizontal movements are prevented, The slenderness ratio adopted 2.15 shows uniaxial behavior at a middle height[Oliveria etal]

7.4.1 Masonry and Interface properties adopted for Brick prism

The Interface stiffness are adopted from CUR report (1997).The following table gives the information about elastic material properties of Brick and Mortar Interface and the stiffness degradations factors are adopted from Oliveria etal[33]

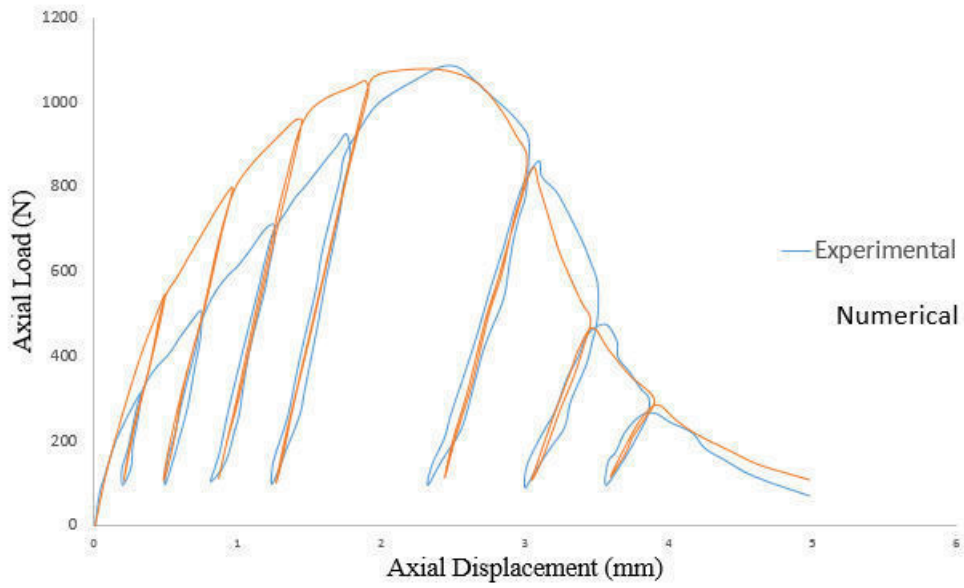


Figure 7.11: comparison between Experimental and proposed Models Numerical results(Oliveria Etal (2005)

	Unit	Interface	
E [N/mm ²]	ν [Poissons ratio]	k_n [N/mm ³]	[N/mm ³]
14700	0.20	648	288

Figure 7.12: Mateial Parameters adopted for Brick and Interface (Oliveria etal)

$\frac{\kappa_1}{\kappa_e}$	$\frac{\kappa_2}{\kappa_e}$	$\frac{\Delta \kappa_e}{\kappa_e}$
0.71	0.05	0.02

Inelastic Parameters for interface adopted to include stiffness degradation

Figure 7.13: Degradation parameters adopted for MortarInterface Oliveria Etal

7.5 Summary and Conclusions

The complex cyclic behavior of Masonry is studied and a Plasticity based approach is followed to simulate the cyclic behavior of Unreinforced Masonry and a Model is proposed to include nonlinearity that accounts for degradation of stiffness in cyclic loading cases . More accurate simulation of Nonlinearity can be achieved depending on the Hardening laws adopted ,however exact reproduction of experimental behaviour is not the aim ,So a good agreement between Experimental and numerical results has been achieved in the Uniaxial Cyclic compression case

Chapter 8

References

8.1 References

1. Continuum Model for Masonry: Parameter estimation and Validation By Paulo B. Lourenco Jan G. Rots, 2 and Johan Blaauwendraad J journal of engineering structures
2. Oliveira DV. Experimental and numerical analysis of blocky masonry structures under cyclic loading. PhD. Dissertation, Universidade do Minho, Guimarães, Portugal, 2003.
(also available at www.civil.uminho.pt/masonry)
3. In-Plane Experimental Behavior of Stone Masonry Walls under Cyclic Loading
G. Vasconcelos and P. B. Lourenço 10.1061/ ASCE ST.1943-541X.0000053
4. (Nonlinear response of masonry wall structures subjected to cyclic and dynamic loading José Fernando Sima, Pere Roca, Climent Molins Engineering Structures 33 (2011) 1955,1965)
5. In-plane shear behaviour of unreinforced masonry walls 14 ECEE2010(S. Churilov, E. Dumova-Jovanoska)
6. Rigid element model for in-plane dynamics of masonry walls (Siro Casolo¹, and Fernando Pena (2007) considering hysteretic behaviour and damage) EARTHQUAKE ENGINEERING AND STRUCTURAL DYNAMICS Earthquake Engng Struct. Dyn. 2007; 36:1029?104
7. (Pan Y-W. Generalized nonassociative multisurface approach for granular materials. J Geotech Eng ASCE 1991;117(5):1336?53)
8. Dolatshahi KM, Aref AJ. Two-dimensional computational framework of mesoscale rigid and line interface elements for masonry structures. Eng Struct
9. Karapitta L, Mouzakis H, Carydis P. Explicit finite-element analysis for the inplane cyclic behavior of unreinforced masonry structures. Earthquake Eng Struct Dyn 2011;40:175?93. 2011;33:3657?67
10. A three-dimensional cyclic meso-scale numerical procedure for simulation of unreinforced masonry structures Amjad J. Aref ?, Kiarash M. Dolatshahi Computers and Structures 120 (2013) 9?23)
11. Compartimento della muratura dal punto di vista materiale e strutturale: simulazioni con un codice di calcolo commerciale
12. Modelling of historical masonry structures: comparison of different approaches through a case study A. Giordano, E. Mele, A. De Luca
Structural Analysis and Design Department (DAPS), University of Naples 'Federico II', P.le Tecchio 80, 80125 Naples, Italy

13. P. Schubert. Tensile and flexural strength of masonry: influences, test methods, test results. In Proc. 10th Int. Brick and Block Masonry Conf. 1994 895–907.
14. R. Van der Pluijm. Material properties of masonry and its components under tension and shear. In Proceedings of the 6 th Canadian Masonry Symposium. Saskatoon, Saskatchewan: University of Saskatchewan. 1992 .
15. R. Pluijm. van der.(1993). Shear behaviour of bed joints. In Proc. 6th North American Masonry Conf., Drexel University, Philadelphia, Pennsylvania, USA .
16. R. Atkinson, B. Amadei, S. Saeb, and S. Sture. Response of masonry bed joints in direct shear. *Journal of Structural Engineering* 115, (1989) 2276–2296.
17. L. Pel'a, A. Aprile, and A. Benedetti. Seismic assessment of masonry arch bridges. *Engineering Structures* 31, (2009) 1777–1788.
18. Dhanasekar, M., and Page, A.W., 1986, "The influence of brick masonry infill properties on the behavior of infilled frames." *Proceedings of the Institute of Civil Engineers* , Part 2, 81, Dec., 593-605.
19. Dhanasekar, M., Kleeman, P.W., and Page, A.W., 1985, "Biaxial Stress-Strain Relation for Brick Masonry." *Journal of Structural Engineering* , ASCE, 111(5), May.
20. A. Zucchini and P. Lourenço. A micro-mechanical model for the homogenisation of masonry. *International Journal of Solids and Structures* 39, (2002) 3233–3255.
21. A. Zucchini and P. B. Lourenço. A micro-mechanical homogenisation model for masonry: Application to shear walls. *International Journal of Solids and Structures* 46, (2009) 871–886.
22. L. Gambarotta and S. Lagomarsino. Damage models for the seismic response of brick masonry shear walls. Part I: the mortar joint model and its applications. *Earthquake engineering structural dynamics* 26, (1997) 423–439.
23. L. Gambarotta and S. Lagomarsino. Damage models for the seismic response of brick masonry shear walls. Part II: the continuum model and its applications. *Earthquake engineering structural dynamics* 26, (1997) 441–462.
24. A. Anthoine. Derivation of the in-plane elastic characteristics of masonry through homogenization theory. *International Journal of Solids and Structures* 32, (1995) 137–163.
25. A. Anthoine. Derivation of the in-plane elastic characteristics of masonry through homogenization theory. *International Journal of Solids and Structures* 32, (1995) 137–163.
26. A. Urbanski, J. Szarlinski, and Z. Kordecki. Finite element modeling of the behavior of the masonry walls and columns by homogenization approach. *Computer methods in structural masonry* 3, (1995) 32–41.
27. Cundall PA. Formulation of a three-dimensional distinct element model. Part I: a scheme to detect and represent contacts in a system composed of many polyedral blocks. *Int J Rock Mech* 1988;25:107–16.
28. Cundall PA. A computer model for simulating progressive large scale movements in blocky rock systems. In: *Proceedings of the Symposium of the International Society of Rock Mechanics*, vol. 1, paper II-8, Nancy (France), 1989
29. Atkinson RH, Amadei BP, Saeb S, Sture S. Response of masonry bed joints in direct shear. *J. Struct. Eng. ASCE* 1989; 115(9): 2276-2296.
30. Stankowski T, Runesson K, Sture S. Fracture and slip of interfaces in cementitious composites. I: characteristics. *J. Eng. Mech. ASCE* 1993; 119(2): 292-314.
31. Jefferson AD, Mills NR. Fracture and shear properties of concrete construction joints from core

samples. *Materials and Structures* 1998; 31: 595-601.

32. Lourenço, P.B. Ramos LF. Characterization of the cyclic behavior of dry masonry joints. *J. Struct. Eng. ASCE* 2004; May (accepted for publication).

33. Implementation and validation of a constitutive model for the cyclic behaviour of interface elements D.V. Oliveira , P.B. Lourenço Department of Civil Engineering, University of Minho, Azurém, 4800-058 Guimarães, Portugal

34. Plasticity based approach for failure modelling of unreinforced masonry Nitin Kumar, Amirtham Rajagopal, Manoj Pandey